applied sciences

MDPI

Article

Understanding the Origin and Mixing of Deep Fluids in Shallow Aquifers and Possible Implications for Crustal Deformation Studies: San Vittorino Plain, Central Apennines

Marino Domenico Barberio [1], Francesca Gori [1], Maurizio Barbieri [1], Tiziano Boschetti [2], Antonio Caracausi [3], Giovanni Luca Cardello [4] and Marco Petitta [1,*]

[1] Earth Sciences Department, Sapienza University of Rome, 00185 Rome, Italy; marinodomenico.barberio@uniroma1.it (M.D.B.); francesca.gori@uniroma1.it (F.G.); maurizio.barbieri@uniroma1.it (M.B.)
[2] Department of Chemistry, Life Sciences and Environmental Sustainability, University of Parma, 43124 Parma, Italy; tiziano.boschetti@unipr.it
[3] National Institute of Geophysics and Volcanology, 90146 Palermo, Italy; antonio.caracausi@ingv.it
[4] Department of Chemistry and Pharmacy, University of Sassari, 07100 Sassari, Italy; glcardello@uniss.it
* Correspondence: marco.petitta@uniroma1.it; Tel.: +39-064991-4834

Abstract: Expanding knowledge about the origin and mixing of deep fluids and the water–rock–gas interactions in aquifer systems can represent an improvement in the comprehension of crustal deformation processes. An analysis of the deep and meteoric fluid contributions to a regional groundwater circulation model in an active seismic area has been carried out. We performed two hydrogeochemical screenings of 15 springs in the San Vittorino Plain (central Italy). Furthermore, we updated the San Vittorino Plain structural setting with a new geological map and cross-sections, highlighting how and where the aquifers are intersected by faults. The application of Na-Li geothermometers, coupled with trace element and gas analyses, agrees in attributing the highest temperatures (>150 °C), the greatest enrichments in Li (124.3 ppb) and Cs (>5 ppb), and traces of mantle-derived He (1–2%) to springs located in correspondence with high-angle faults (i.e., S5, S11, S13, and S15). This evidence points out the role of faults acting as vehicles for deep fluids into regional carbonate aquifers. These results highlight the criteria for identifying the most suitable sites for monitoring variations in groundwater geochemistry due to the uprising of deep fluids modulated by fault activity to be further correlated with crustal deformation and possibly with seismicity.

Keywords: groundwater mixing; deep fluids; earthquake-hydrology; isotope; geochemistry

Citation: Barberio, M.D.; Gori, F.; Barbieri, M.; Boschetti, T.; Caracausi, A.; Cardello, G.L.; Petitta, M. Understanding the Origin and Mixing of Deep Fluids in Shallow Aquifers and Possible Implications for Crustal Deformation Studies: San Vittorino Plain, Central Apennines. *Appl. Sci.* **2021**, *11*, 1353. https://doi.org/10.3390/app11041353

Academic Editor: Dibyendu Sarkar
Received: 7 December 2020
Accepted: 26 January 2021
Published: 3 February 2021

1. Introduction

Groundwater hydrogeochemistry is closely related to the nature of the aquifer and to the length and depth of the groundwater flow paths, and it strongly depends on the residence time [1,2]. However, structural-geological features (e.g., faults and the tectonic pattern distribution) can also affect the water chemistry, as they allow and facilitate the mixing of groundwater of different origins [3,4]. While down-going fluids may be of meteoric (or even karstic) origin, uprising fluids may connect the lowermost parts of a stratified aquifer to the surface. Direct field evidence of exhumed seismogenic zones in carbonate rocks furnishes a fossilized example of how high pore-fluid pressure currently is at depth [5,6]. In these contexts, the vein and fault record demonstrated that isotopic equilibrium can be interrupted during exhumation by transient thoroughgoing faulting, allowing meteoric fluids to reach otherwise rock-buffered fluid systems [7–9]. Additionally, deep fluids play an active role in the seismic cycle and fault activation mechanisms, which are increasingly highlighted in geoscience studies [10–18]. For this reason, in recent decades, works aimed at identifying signals that can anticipate strong seismic events in field and laboratory activities have been intensified [3,19–25]. These studies have

identified variations in the concentration of gases such as He, Rn, CO_2, H, and CH_4 [26,27], groundwater chemical content [3,21,22], and the physical properties of rocks [28,29].

However, determining the origin of fluids in shallow aquifers and answering the questions of where and how these fluids originate, and determining the possible water–gas–rock interaction processes during their migration, can provide new constraints for understanding the processes related to seismogenic processes. Research in this direction has mainly deepened the understanding of fluid origins, focusing on the determination of quantities useful to define their origin and mixing. In detail, some conservative elements in waters (e.g., As, V, Fe, Li, Cs, and Rb) and isotopes of some gaseous species (e.g., He and Ar) have been recognized and used as tracers that are often not bound to a circulation model [21,30–33]. In this frame, the central Apennines mountain belt in central Italy represents a natural laboratory to efficiently examine these topics, both for its tectonic-structural framework [34], the abundance of groundwater resources [35], and the rise of deep fluids along normal faults [11–13,36,37].

In addition, the nature of the regional aquifers hosted by fractured Meso–Cenozoic carbonates with limited karst development [38] enhances the response to deep fluids uprising through the shallow crustal layers, possibly allowing fast and concentrated changes in groundwater close to high-angle faults, coupled with smoothed and aquifer-wide less evident effects on hydrogeochemistry. Thus, to improve the comprehension of the relationships of both deep and shallow fluids in regional aquifers, we conducted an integrated study of the regional hydrostructures and water composition in the San Vittorino Plain, an intramontane basin in the central Apennines. In fact, this plain is characterized by an abundance of water resources [38,39] and large diffuse active degassing focused along high-angle faults [36]. Overall, the area is defined by different fault systems related to the different steps of the regional structural history [40], and there are traces of Quaternary volcanism [41,42]. In addition, according to a recent study [37] which aimed to evaluate the aquifer's potential susceptibility to be affected by detectable chemical-physical anomalies during seismogenic processes, the San Vittorino Plain has been placed at the "top-ranking position" as one of the most suitable areas for the monitoring of seismic activity in central Italy by groundwater monitoring.

By sampling and analyzing 15 springs with different degrees of mineralization and gaseous contents, combined data of the chemical composition (chemical-physical parameters, major and minor elements, and free and dissolved gases), isotopic ratios ($\delta D/\delta^{18}O$-H_2O, $\delta^{13}C$-CO_2, He, and Ar), and Na/Li geothermometry were used to establish first the origin and then the mixing extent of the deep and shallow fluids into the San Vittorino Plain aquifers. We investigated the role of thermodynamic balance, established among gas, water, and rock, and the secondary processes that influence aquifer chemistry, providing new insights for understanding hydrogeochemical variations as a function of crustal deformations in the framework of a well-known hydrogeological conceptual model [38,43].

In summary, the aim of this research was to improve the comprehension of the mechanisms of deep fluid rise and mixing in large regional aquifers to better understand: (i) the role of the different local fault systems and regional crustal structures in spreading deep fluids in aquifers and related springs; and (ii) the identification of criteria for establishing useful groundwater monitoring of the changes in mixing of these fluids with time and space as a function of crustal deformation and, consequently, their correlation with micro- and possibly macro-seismicity of the area.

2. Geological and Hydrogeological Setting

2.1. Apennines Tectonics Summary

The fold-and-thrust belt structure between the northern and central Apennines has developed since the Oligocene, with a main east to northeastward vergence (Figure 1) [34,44–46]. Generally, the carbonate domains of the Apennines were affected during the late Triassic, early Jurassic, and early Cretaceous by syn- to late-rift tectonic effects, which determined sedimentary successions with long-living platforms to the east of the study area and the

basinal domains to the west and north of it [47,48]. The Reatini Mountains (Mts) are composed of Mesozoic carbonate pelagic successions (basinal units), while the Giano Mt. and Nuria Mt. are made of thick shallow water carbonate successions (Figure 1). During the late Cretaceous, shallow water platforms were further fragmented and drowned at their rims. Until the early Miocene, this allowed the deposition of basinal to escarpment sediments (e.g., Navegna Basin, Figure 1). In the middle Miocene, outer to inner carbonate ramp units were deposited on the different downstepped blocks that were then invaded by thick synorogenic successions during the late Miocene [49]. Further, during the late Miocene orogenic phase, these units piled up towards East-North-East in the fold-thrust belt [50]. The postorogenic extensional tectonics and erosion started from the Pliocene and are still ongoing [51,52]. This crustal regime enhanced the development of intramontane plains and alluvial valleys among the carbonate ridges (Figure 1) [53]. The deep structure of the study area is poorly constrained due to the scarcity of available wells and absence of seismic lines, and the uncertainty of the thickness and continuity of the structural units.

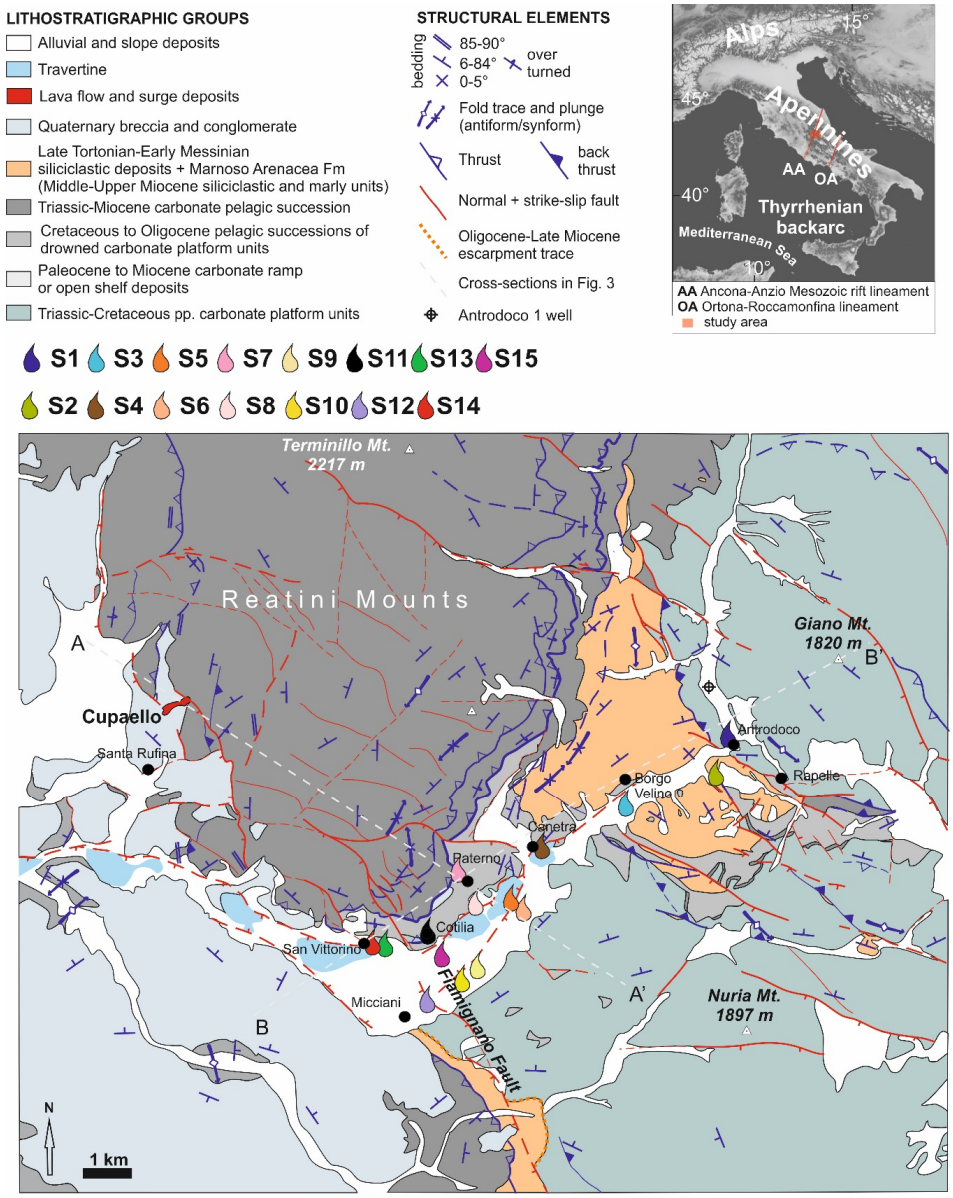

Figure 1. Simplified tectonic map of the study area modified after the compared review of Foglio "L'Aquila" and "Rieti" (https://www.isprambiente.gov.it/ accessed on 3 February 2021) [40,49,50,54,55]. The map shows the location of the selected springs.

2.2. The San Vittorino Plain Structure

The San Vittorino Plain is one of the intramontane basins of the Apennines (elevation of 400–425 m a.s.l.) and is defined as a complex graben with a length of approximately 4 km and a width of approximately 2 km, hosting the Velino River. The plain is located between the Latium–Abruzzi neritic carbonate platform domain (Giano Mt. and Nuria Mt. ridge, on the east; Figure 1) and the Umbria–Marche–Sabina basinal domain on the west (Reatini Mounts) [39,40]. The area has recorded regional polyphase tectonic activity. In particular, traditionally, the Ancona–Anzio lineament ([56,57] and references therein) was reactivated during the late Miocene as a transpressive front that subdivides the northern from the central Apennines (i.e., the Olevano–Antrodoco–Sibillini line) [58]. These factors allowed the basinal domain to overthrust the platform together with its late Miocene synorogenic deposits (e.g., siliciclastic deposits). The fold-and-thrust structure was later affected by regional uplift and was passively cross-cut by Quaternary transtensive structures allowing the sedimentation of thick lower-middle Pleistocene breccia and conglomerates within tight continental graben-like basins [46,59–61]. Lateral and vertical heteropic stratigraphic contacts occur within the clastic deposits of the plain subsoil, while several fault systems define the tectonic network in this area [40] (Figure 1). Among these faults, the Fiamignano Fault is one of the most relevant normal faults and related paleoescarpments. It trends NW–SE and dips to the SW (Figure 1), showing polyphase activity during the Cenozoic and later also during the Quaternary [40,47,49]. Further, NE-striking faults occur in the San Vittorino Plain, downthrowing the Meso–Cenozoic carbonates in the graben. Nearly N-striking transtensive faults occur at the western edge of the Reatini Mounts, bounding continental clastic successions. Near their top, the Cupaello eruptive center (melilititic ultrapotassic kamafugites and carbonatites: the last activity 0.64 Myr ago; Figure 1), occurs at a major fault [41,42].

2.3. Hydrogeological Setting

The carbonate ridges in the central Apennines correspond to wide recharge areas of the main fractured regional aquifers that can store large quantities of groundwater. Groundwater flow in fractured carbonate aquifers is laterally limited by continental depositional sequences in the intramontane plains, and tectonic activity induces continuous base-level changes in the aquifers [39,62]. These conditions have possibly hindered the development of a mature karst network in the discharge areas of the aquifers [63]. Therefore, in such wide aquifers (up to 1000 km^2), an impulsive response to seasonal recharge is not recognizable, as stated by very high and steady spring discharges [39], located at the boundaries of the carbonate aquifers limited by recent clastic and alluvial deposits. The San Vittorino Plain hosts the discharge of large carbonate aquifers; for example, the Giano–Nuria–Velino Mts hydrogeological system [38,39] (Figure 1). These fractured ridges, belonging to the carbonate platform domain, are highly permeable due to fracturing and karst processes in the recharge zone, with a total recharge area of approximately 1016 km^2, and effective infiltration of 880 mm/yr vs. the average precipitation of over 1200 mm/yr [35,64]. These carbonate aquifers feed spring groups with a total discharge of approximately 30 m^3/s [39]. The main springs are located on the southern and northern boundaries of the San Vittorino Plain and include the Peschiera springs (S10 (Figure 1), 18 m^3/s), partially exploited for drinking purposes; the streambed springs of Antrodoco (approximately 2 m^3/s), the spring group of Canetra (S4, 4.5 m^3/s), San Vittorino (S14, 0.5 m^3/s), and the highly mineralized springs of Terme di Cotilia (S11, 0.25 m^3/s). On the other hand, the Paterno perched spring, located on the right slope of the Velino River, is fed by the Mt. Paterno–Canetra ridge (S7, Figure 1). This minor hydrogeological unit also contributes to regional groundwater recharge.

In addition, spring locations and hydrogeochemistry are influenced by tectonics and the different permeabilities of the alluvial/clastic layers of the plain, having variable widths, up to approximately 200 m. Groundwater from carbonate aquifers can undergo chemical-physical variations upon its transfer towards the alluvial shallow aquifer. Consequently,

the springs of the area have different hydrogeochemical characteristics that are also the result of active degassing in the middle valley of the Velino River [31,36,38,39,43,65]. Hence, mixing induced by deep fluid inputs, whose upward movements occur along tectonic discontinuities and are partially buried by recent clastic deposits, may cause progressive and significant hydrogeochemical changes in the springs.

Although the San Vittorino Plain is far from having any evidence of active volcanism, it is characterized by relevant gas emissions, with a maximum CO_2 flux of 5.7×10^{-5} kg m^{-2} d^{-1} [31,38,66]. In some cases, the aggressiveness of the waters conferred by gaseous contributions can promote the development of collapse phenomena, so-called sinkholes [67]. Through the assessment of the chemical composition of the fluids associated with the sinkholes of the plain, the origin of this CO_2 was explained as being the combination of both a mantle source and a product of thermometamorphic reactions within the buried Meso–Cenozoic limestone [68].

3. Methods

3.1. Sampling and Analysis

To characterize the hydrogeochemistry of groundwater in the study area, 15 of the most representative springs with different geochemical features were selected (e.g., from low to high mineralization, the presence and/or absence of free gases and bubbling) from among approximately 80 springs measured in previous studies [39]. Water samples were collected during two surveys performed in October 2018 and January 2019. In each sampling campaign, chemical-physical parameters (temperature, pH, and electrical conductivity) were also measured on-site through the multiparametric probe WTW Multi 3620 IDS.

The collected samples for several analyses (including major and trace elements, stable isotope of water, dissolved and free gases, and noble gas isotope ratio) were kept at low temperatures in ice-filled fridge boxes to avoid alterations of components prior to the laboratory analyses. Samples for the determination of major (anions and cations) and trace element concentrations were analyzed at the Geochemistry Laboratory of Earth Sciences Department of Sapienza University (Rome, Italy). Samples for analysis of the stable isotopes (δ^{18}O-H_2O and δD-H_2O), gaseous contents, and isotopic ratios were sent to the geochemistry laboratories of the National Institute of Geophysics and Volcanology of Palermo.

Samples for the major and trace element analyses were filtered in situ through a 0.45 µm filter into polyethylene bottles. In addition, waters collected for trace element analysis were acidified with added concentrated ultrapure HNO_3 to prevent the precipitation of metals. Samples for the analyses of stable isotopes and dissolved gases were collected in glass bottles. Gas samples were collected in Pyrex bottles with vacuum valves at both ends, taking care to prevent air contamination.

For the determination of major ions, samples were analyzed by ion chromatography. Waters with a high electrical conductivity (greater than 800 µS/cm) were diluted with ultrapure water before inserting them into the chromatograph.

To determine the anionic content (F^-, Cl^-, SO_4^{2-}, and NO_3^-), a Dionex ICS 5000 chromatograph was used, while the cationic content (Ca^{2+}, Mg^{2+}, Na^+, and K^+) was determined by a Dionex ICS 1100 chromatograph. The analytical error associated with these instruments is less than 5%, as also testified by the cation–anion balance checked on each sample [69]. The software Dionex Chromeleon, connected to both chromatographs, allowed us to know the concentrations of each major ion of the sampled waters in terms of ppm (mg/L). Alkalinity was measured by titration with 0.05 N HCl on site.

Analysis of the trace elements was carried out using an ICP-MS spectrometer (X Series 2 Thermo Fisher Scientific Waltham, MA, USA). Ultrapure water (Millipore, Milli-Q, 16 MΩ cm) was used to prepare blanks, standard solutions, and sample dilutions, and an internal standard, Rh, was added to correct the ICP-MS instrumental drift. The analytical accuracy of this method ranges between 2% and 5% [21,70].

Measurement of the stable isotopes of water ($\delta^{18}O$ and δD) was carried out on samples collected in the first campaign (October 2018) to improve the hydrogeochemical model and to understand the mixing processes between the waters of the regional karst system and those of deep origin. These analyses were performed at the Istituto Nazionale di Geofisica e Vulcanologia of Palermo, Sicily, Italy.

The isotopic ratio of oxygen was measured using a Thermo Delta V Plus mass spectrometer coupled to a GasBench II, exploiting the equilibration technique between H_2O and CO_2 [71]. For the determination of the hydrogen isotopic ratio, a Delta Plus XP mass spectrometer coupled with a TC/EA reactor was utilized. The isotopic values for the waters are expressed in δ‰ vs V-SMOW (Vienna Standard Mean Oceanic Water). The uncertainties were ± 0.1% for $\delta^{18}O$ and ± 1% for δD. A fast and completely automated procedure to determine the $\delta^{13}C$ (as V-PDB, Vienna Pee Dee Belemnite) of total inorganic carbon dissolved in water ($\delta^{13}C_{DIC}$) was utilized [72]. This method is based on the acidification of water samples transforming the whole dissolved inorganic carbon species into CO_2. Water samples are directly injected with a syringe into vials with screw caps that have a pierceable rubber septum. A GasBench II was used both to flush pure helium into the vials and to automatically dispense a fixed amount of H_3PO_4. Full-equilibrium conditions between the produced CO_2 and water are reached at a temperature of 70 °C (± 0.1 °C) in less than 24 h. Carbon isotope ratios ($^{13}C/^{12}C$) were measured on a Delta V Plus mass spectrometer connected online with GasBench II.

The dissolved gas content was determined with a gas chromatograph (Perkin Elmer 8500) with an Ar carrier on a 4 m column (Carbosieve SII) and double detector (TCD and FID – Thermal and Flame Ionization Detector, respectively) [73]. The analytical error was evaluated to be approximately ± 3% for all gaseous species. Based on the solubility data of gaseous species in water, the concentrations of the dissolved gases in the water were calculated [74] and also corrected for atmospheric contamination, taking into account the N_2/O_2 ratio in the samples and comparing it with the same ratio in the atmosphere.

He isotopes were analyzed with a static vacuum mass spectrometer (GVI Helix SFT), characterized by a double collector that allows the simultaneous detection of the ^3He and ^4He ion beams (isotopic precision ratio within ± 0.5%). The $^3He/^4He$ ratio was obtained by measuring ^3He and ^4He in an electron multiplier detector and in an axial Faraday detector, respectively. Ne isotopes were measured by a multi-collector mass spectrometer (model Thermo-Helix MC plus) after standard purification procedures ([17] and references therein). He isotopic ratios are reported as R/Ra values, where Ra is the He-isotope ratio in the atmosphere (1.39×10^{-6}). Overall, analyses of gases (free, dissolved, and isotopes) were provided in the noble gases laboratory at the Istituto Nazionale di Geofisica e Vulcanologia of Palermo.

3.2. Thermodynamic and Isotopic Calculations

The mineral saturation indices and the partial pressure of dissolved carbon dioxide as $\log P(CO_2)$ were calculated using the PHREEQC Interactive code (PHREEQCi version 3) and the llnl.dat/thermo.com.v8.dat thermodynamic databases [75]. To check the uncertainty related to different data sets and calculation methods of the activity coefficients (i.e., Debye–Hückel, B-Dot), the parameters for selected samples with the Spec8 tool of The Geochemist's Workbench's® code (release 12) [76] and the thermo.dat thermodynamic datasets were also calculated. The same codes were used to calculate the molality of the so-called C_{ext} parameter, i.e., the carbon from external sources derived from processes other than the interaction with carbonate rocks (C_{carb}) [33,77]. In addition, to evaluate the $\delta^{13}C$ isotope composition of CO_2 ($\delta^{13}C_{ext}$) in the inspected water samples [33], the NetpathXL 1.5 code was used [78,79]. The input data for this latter code were the $\delta^{13}C_{DIC}$ values, chemical-physical parameters (pH, T) and chemical composition of the water samples. During calculation, the value of $\delta^{13}C_{carb}$ = +2.2‰ was assumed to be the isotopic composition of the carbonate aquifer [80,81]. The obtained $\delta^{13}C_{ext}$ results are substantially the same if we also take into account the difference in the isotope composition of the Mesozoic

carbonate minerals in the Antrodoco area [82]: $\delta^{13}C_{dolomite}$ = +2.7‰ and $\delta^{13}C_{calcite}$ = +1.6‰. However, in comparison with the similar approach of [36], the $\delta^{13}C_{ext}$ calculated by Netpath showed an enrichment of approximately +1.13 ‰, because the code takes into account the fractionation effect related to carbon dioxide solubilization: $CO_2(g) \rightarrow CO_2(aq)$ [33]. Finally, the statistical significance of the ordinary least square (OLS) regressions was checked using both the OriginLab code [83] and the table of critical values for Pearson's r correlation coefficient from the N parameter (two-tailed test).

3.3. Map Review and Cross-Section Construction

The lithostratigraphic architecture of the carbonate succession has been reviewed into a new geological map (Figure 1) that was produced after the grouping of the different lithostratigraphic units reported in the ISPRA dataset and in the literature [49,50,54,84]. We have thus harmonized the stratigraphic and tectonic information published in the 1:100,000 maps (L'Aquila, Rieti; https://www.isprambiente.gov.it/ accessed on 3 February 2021), and we also considered the distribution of the Quaternary deposits [55].

To build the geological cross-sections, bibliographic and available stratigraphic information were compared. The basal decollement was extrapolated from the position of the evaporites in [84]. Cross-sections were drawn perpendicular to the main direction of transport during convergence and subparallel to the strike to provide a 3D sketch overview of the deep circulation of the fluids. The thickness of the units is virtually constant. The attitude of the layers at the surface guides the interpretation of the deeper structures. The Antrodoco 001 well stratigraphy has been reported, as it is available from a public data set (available online: https://www.videpi.com accessed on 3 February 2021).

4. Results

The 15 sampled springs are characterized by moderate to high salinity. The hydrogeochemical facies are Ca-HCO_3 and Ca-SO_4 types [38,39,43]. In addition, some springs show continuous bubbling of free gases [31,68].

4.1. Hydrogeochemical Results: Chemical-Physical Parameters, Major and Trace Elements, and H_2O Stable Isotope Ratio

The chemical-physical parameters (e.g., temperature, pH, and electrical conductivity) and trace element concentrations of each survey are presented in Supplementary File Table S1.

The Piper diagram [85] (Figure 2) shows two main hydrogeochemical facies. As expected, waters are predominantly enriched in bicarbonate and calcium ions (Ca-HCO_3 facies). The freshwater endmember is represented by S7. The other springs, despite showing the same hydrogeochemical facies, are progressively enriched in SO_4 and Mg. This condition is attributable to the increase in the water–rock interaction due to the flow path in the main aquifer and/or the progressive mixing with groundwater that has different chemical compositions. Only springs of the Antrodoco area (i.e., S1 and S2) are included in the calcium-sulphate waters domain (Ca-SO_4 facies). This evidence suggests the circulation of this groundwater in Triassic carbonate-evaporitic formations and limited dilution with Ca-HCO_3 water.

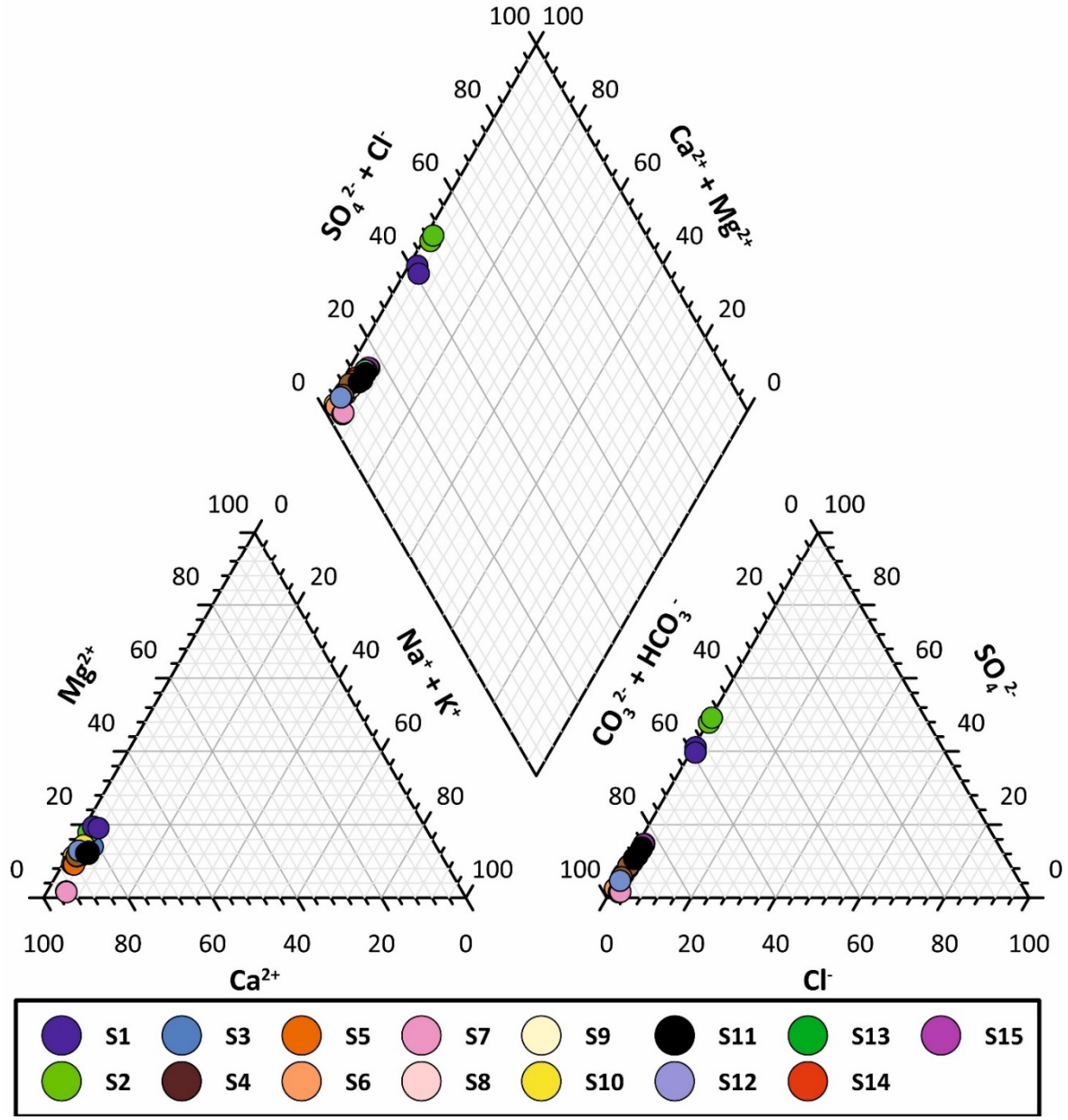

Figure 2. Piper diagram of groundwater samples from the San Vittorino Plain. All samples are predominantly enriched in bicarbonate and calcium ions (fresh waters and mixing waters; Ca-HCO_3 facies). Only springs of the Antrodoco area (i.e., S1 and S2) are included in the calcium-sulphate waters domain (mineralized waters; Ca-SO_4 facies). For spring location see Figure 1.

Stable isotopic analyses of water sampled in October 2018 were carried out to investigate their origin and groundwater flow paths, as well as to eventually determine the physical processes and chemical reactions that take place during groundwater flow. The springs are characterized by isotopic values from −8.9 to −9.8‰ and from −53 to −62‰ for $\delta^{18}O$ and for $\delta^{2}H$, respectively (see Supplementary File Table S1).

4.2. Gas Geochemical Results: Dissolved and Free Gases, Noble Gas, and Isotope Ratio

The collected samples refer to both free and dissolved gases depending on the presence/absence of bubbling in the water of selected springs in each survey. Only four samples for free gases were taken in January 2019.

The results of the performed gas analyses (both free and dissolved gases) are reported in Supplementary File Table S1. Almost all water samples are CO_2 dominated with

concentrations ranging from 3.1 to 663.7 ccSTP/L. Some springs (e.g., S3, S6, and S12) recorded concentrations that were lower than the detection limit. Similarly, CH_4 was also measured only in some springs (Supplementary File Table S1) with concentrations between 5.21×10^{-5} and 1.52×10^{-3} ccSTP/L. Helium concentrations vary from 3.19×10^{-4} to 3.92×10^{-3} ccSTP/L. He-isotope composition in the collected fluids ranges from 0.07 Ra to 0.15 Ra. The $^{4}He/^{20}Ne$ ratios of all investigated fluids are generally higher than 0.318 (i.e., the value of the atmosphere) [86], indicating that air contamination was negligible [73]. The only exception is the sample collected at S11, in which $^{4}He/^{20}Ne$ is lower than 1, showing that this sample is affected by air contamination. All the samples have $^{40}Ar/^{36}Ar$ ratios that are indistinguishable from the ratio in the atmosphere.

4.3. Deep Structural Interpretation

In light of our structural review, we hereby present two geological cross-sections (Figure 3), aiming at providing a structural sketch for the possible paths of fluid circulation within the studied complex aquifer down to a depth of approximately 5–6 km. Field evidence allows us to trace at depth a persistent Jurassic–Miocene carbonate pelagic succession that crops out in the west and includes Triassic evaporites and dolomites, and early Jurassic fractured and porous carbonates (Reatini Unit). In the east, we also distinguish two Triassic–Cretaceous carbonate platform units (i.e., Nuria Mt and Giano Mt). Additionally, the Reatini Unit is internally affected by several thrusts. The overall structural set is dominated by imbricated thrust sheets that involve pre-existing normal faults (orange lines) with associated syn-sedimentary units of variable thickness and facies distribution. These transitional units consist of Cretaceous to Oligocene pelagic successions with resediments shedding out the platform that deposited on top of drowned carbonate platform units. North of the Nuria Mt., they are further topped by middle Miocene carbonate ramp deposits. More to the SW, the Nuria Mt. succession consists of Paleocene to Miocene open shelf to basinal deposits, possibly deposited onto transitional Mesozoic carbonate units. By inverting the basin structures, thrust tectonics determined the occurrence of a thick thrust zone that displays a transpressive lateral ramp with the overturned Reatini Unit on the hanging wall and the Nuria Unit at its footwall (Figure 3). The transitional units within the thrust zone are further imbricated with tectonic lenses of more competent carbonate units, S/C shear fabrics (schistosity/cisaillement), and folds in the more marly units. The oldest fold-and-thrust structure is further crosscut by two major backthrusts that cross-cut both the pelagic succession and, possibly, the Nuria Mt. (cross-section AA', Figure 3). At Antrodoco, the high-angle contact between the Triassic dolomites and the late Tortonian–early Messinian siliciclastic units is interpreted as being intercepted by the Antrodoco 001 well. This suggests that a major backthrust accompanies the formation of a triangular zone (cross-section BB', Figure 3). Finally, to the southwest and to the west, stepwise segments of the normal oblique faults bound the Reatini Mounts and the Nuria Mt. normal fault systems are characterized by lateral strike deviation and offset reduction to a few hundred meters at the fault tips. In our interpretation, these faults, bounding also the San Vittorino Plain, cross-cut the entire fold-and-thrust structure.

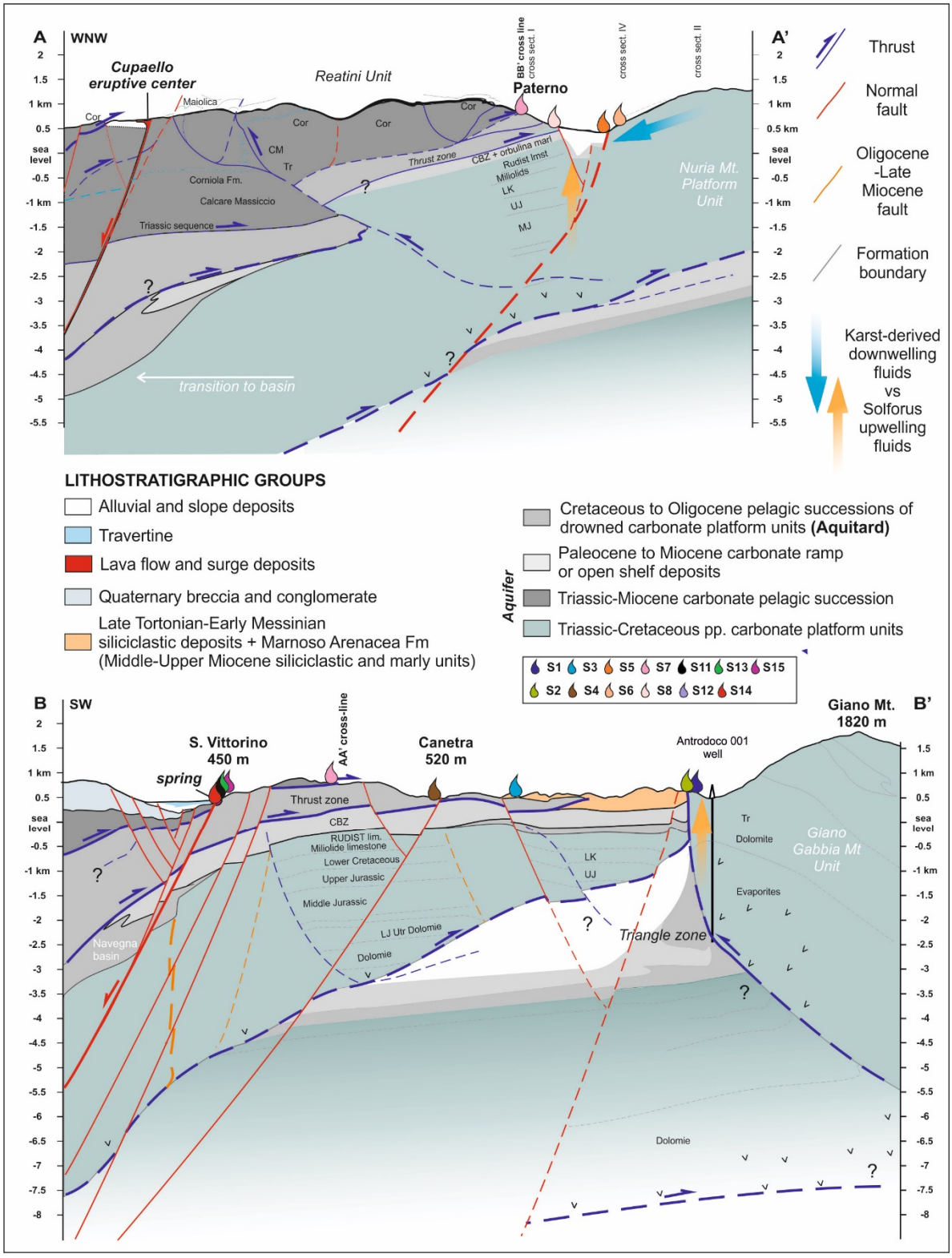

Figure 3. Geological cross-sections showing a sketched reconstruction of the fold-and-thrust belt architecture, which is cross-cut by high-angle transtensive faults. The figure also shows the projection of the Antrodoco 001 well, which intercepts the backthrust tilting the Giano–Gabbia Mt. unit. See Figure 1 for the trace of the cross-sections and relative intersection from [54].

5. Discussion

Previous investigations based on the hydrogeochemistry of the fluids [43,65] highlighted that the groundwater hydrogeochemistry of the San Vittorino Plain is the result of the addition of deep fluids (i.e., mantle-derived and crustal fluids) to the shallow groundwater circulating in a regional carbonate fractured aquifer. All of the selected springs represent the main discharge points and are not affected by surface runoff.

Based on chemical parameters, in the Piper diagram, the groundwater of the 15 selected springs seems to be aligned along a single mixing trend or evolutionary path, whose end-members are Ca-HCO_3 and Ca-SO_4 types (Figure 2). However, a closer look at the bicarbonate corner of the Langelier–Ludwig diagram, which has the same meaning as the central diamond in Piper's plot (Figure S1), reveals at least two possible evolutionary trends: (i) an increase of the sulphate concentration in the Antrodoco area (i.e., S1 and S2) due to dissolution of Upper Triassic gypsum/anhydrite; and (ii) a trend from samples with higher HCO_3 relative concentrations, Peschiera/Paterno areas (S10, S7, S8), towards the S11 and S15 samples. Furthermore, the comparison with the historical data of the selected springs showed that the systematic enrichments of alkali elements Na and K, relative to alkaline earth metals Ca and Mg, occurred in the past (Figure S1) [36,37,43,87–90]. Regardless, the main chemical constituents alone are not enough to explain the hydrogeochemical processes to quantify deep components and their influence on each spring.

With the aim of identifying both chemically and physically the deep fluid end-member, in this paragraph, we will focus on: (i) the reconstruction of thermodynamic balances through the application of different geothermometers; (ii) the study of the possible water–rock interaction processes through the analysis of some conservative elements; (iii) the determination of the origin of free and dissolved gases; and (iv) the connection between deep and shallow aquifer systems through the study of the relationship between the geochemistry of groundwater and neotectonics. Some relevant chemical data are reported in Table 1.

The evaluation of the deep temperature in low enthalpy carbonate-evaporitic systems (T < 150 °C) is frequently a demanding challenge [91]. Regarding central Italy, several approaches using chemical geothermometry have been proposed [91–95]. Recently, the temperatures inferred by the Na-Li ratio offered results consistent with those obtained from multicomponent geochemical models [33]. In this study, the Na-Li inferred temperatures by the [96] equation gradually increase as the contribution of deep inorganic carbon, traceable by the $\delta^{13}C_{ext}$ parameter, increases (Figure 4; Figure S2). Taking into account the absolute uncertainties of this kind of geothermometer (± 20 °C) [96], negative results on waters with shallower circulation in the heterothermic zone of a karst system such as S7 are not as astonishing (Figure 4) [97]. In contrast, most of the spring samples at $\delta^{13}C_{ext} > -5$‰ seem to have a relevant deep contribution and/or circulation in the deep homothermic zone affected by the local geothermal gradient, with a temperature that can be inferred by the Na-Li geothermometer and clustering around the low-high enthalpy limit [33] (T = 150 °C, see Supplementary File Table S1). We did not measure the $\delta^{13}C$(DIC) parameter in some springs (S6, S8, S10, S12, S13, and S15). However, an analysis of historical data reveals how the S10 spring (Peschiera) falls close to the abovementioned $\delta^{13}C_{ext}$ divide of −5‰ ($\delta^{13}C_{ext} = -6.6 \pm 1.2$‰) (Figure 4; Figure S2), confirming the involvement of both shallow and deep fluids [33,36,43,89]. The involvement of a deeper fluid having an increasing amount of CO_2 with a geogenic signature is also confirmed by the significant regression between the Na-Li temperature and the CO_2 partial pressure parameter logPCO_2 calculated under sampling conditions (Figure 5). The SO_4-F geothermometer was adopted to verify the reliability of the results obtained by the Na-Li geothermometer. However, as already found in other geothermal systems [98,99], the SO_4-F geothermometer gave systematically negative temperature values using the equation calibrated for the temperature range of 75–150 °C [95]. Otherwise, the extrapolation of the equation calibrated for the range 150–300 °C [94] offers consistent results with those from Na-Li, but only for the springs showing fewer negative values of the saturation index for gypsum/anhydrite and fluorite.

For example, Antrodoco: T(SO_4-F) = 112 ± 13 °C and T(Na-Li) = 119 ± 14 °C (N = 18). In this study, using the Na-Li temperatures as the most likely temperature at depth and the equations of [94], for S11 (which has a mean T(Na-Li) = 196 ± 25 °C, N = 8), we obtained the highest logPCO_2 = 3.5 value (logPCO_2 = 0.7 ± 0.2 for Antrodoco). Such a relatively high temperature in S11 was also supposed to explain the boron isotope composition of this water that resembles a tourmaline-equilibrated fluid [100]. In contrast, the obtained logPCO_2 values are higher than those obtained with the PHREEQCi code under sampling conditions (Figure 5) but are in the order of magnitude with those of other deep crustal fluids in the Apennine [101]. Therefore, the adoption of the Na-Li geothermometer allowed us to evaluate the temperatures of the San Vittorino system (up to 150–200 °C), where evidence of springs with significant deep contributions was found. Applying the geothermal gradient of the area (66 °C at 3 km depth in the Antrodoco 1 borehole) [102] at these temperatures, an estimation of the depth of fluids ranging between 2.2 and 8.8 km was carried out.

Table 1. Chemical results used in this paragraph. Same spring analyses (location in Figure 1) refer to subsequent samplings.

	Li	Rb	Cs	δ^{13}Cext(g)	Na/Li	log$P(CO_2)$	δD	δ^{18}O	R/Ra	He/Ne	R/Ra	He/Ne
	ppb	ppb	ppb	‰ (vs. V-PDB)	°C		‰ (vs. V-SMOW)	‰ (vs. V-SMOW)	Dissolved	Dissolved	Free	Free
S1	16.46	4.09	1.23	6.38×10^{-1}	125	−0.95	−60	−9.7				
S1	12.50	3.17	0.90	-2.26×10^{0}	86	−1.00			0.11	28.98		
S2	22.73	5.18	1.69	7.86×10^{-1}	144	−0.69	−61	−9.8				
S2	21.20	4.83	1.38	-1.76×10^{0}	127	−0.64			0.11	38.56		
S3	5.60	2.36	0.17		94	−1.34						
S3	4.81	1.53	0.07	-1.71×10^{-1}	58	−1.41			0.08	1.82		
S4	4.95	2.33	0.27	-2.45×10^{0}	94	−1.21	−62	−9.8				
S4	3.96	1.72	0.18	-4.96×10^{0}	80	−1.27			0.10	12.54		
S5	48.73	7.15	7.45	1.93×10^{0}	193	−0.26	−60	−9.8				
S5	47.15	6.54	6.44	-2.51×10^{0}	172	−0.10			0.07	8.35	0.11	121.50
S6	2.81	1.53	0.24		69	−1.18						
S7	0.43	0.58	0.00	-2.00×10^{1}	2	−2.75	−53	−8.9				
S7	0.35	0.60	0.00	-2.81×10^{1}	−5	−2.98						
S8	9.32	2.61	1.10		112	−1.44	−61	−9.8				
S9	1.88	1.38	0.07	-3.37×10^{0}	52	−0.92			0.12	9.12	0.17	20.57
S10	1.53	1.53	0.06		48	−1.68	−60	−9.8				
S11	98.11	9.64	5.36	2.14×10^{0}	193	0.00	−55	−9				
S11	83.65	7.82	3.78		179	−0.19			0.08	0.59		
S11	100.70	9.66	5.14	6.44×10^{0}	148	−0.07					0.10	198.57
S12	5.86	2.29	0.27		99	−1.12						
S13	68.46	7.82	2.02		160	−0.21						
S14	19.81	3.32	0.62	-8.44×10^{-1}	133	−0.76	−59	−9.7				
S14	8.28	1.92	0.49	-3.69×10^{0}	100	−1.12			0.10	13.27	0.15	37.97
S15	105.30	10.45	5.08		167	0.02						
S15	124.30	11.16	5.98		184	0.02	−59	−9.4				

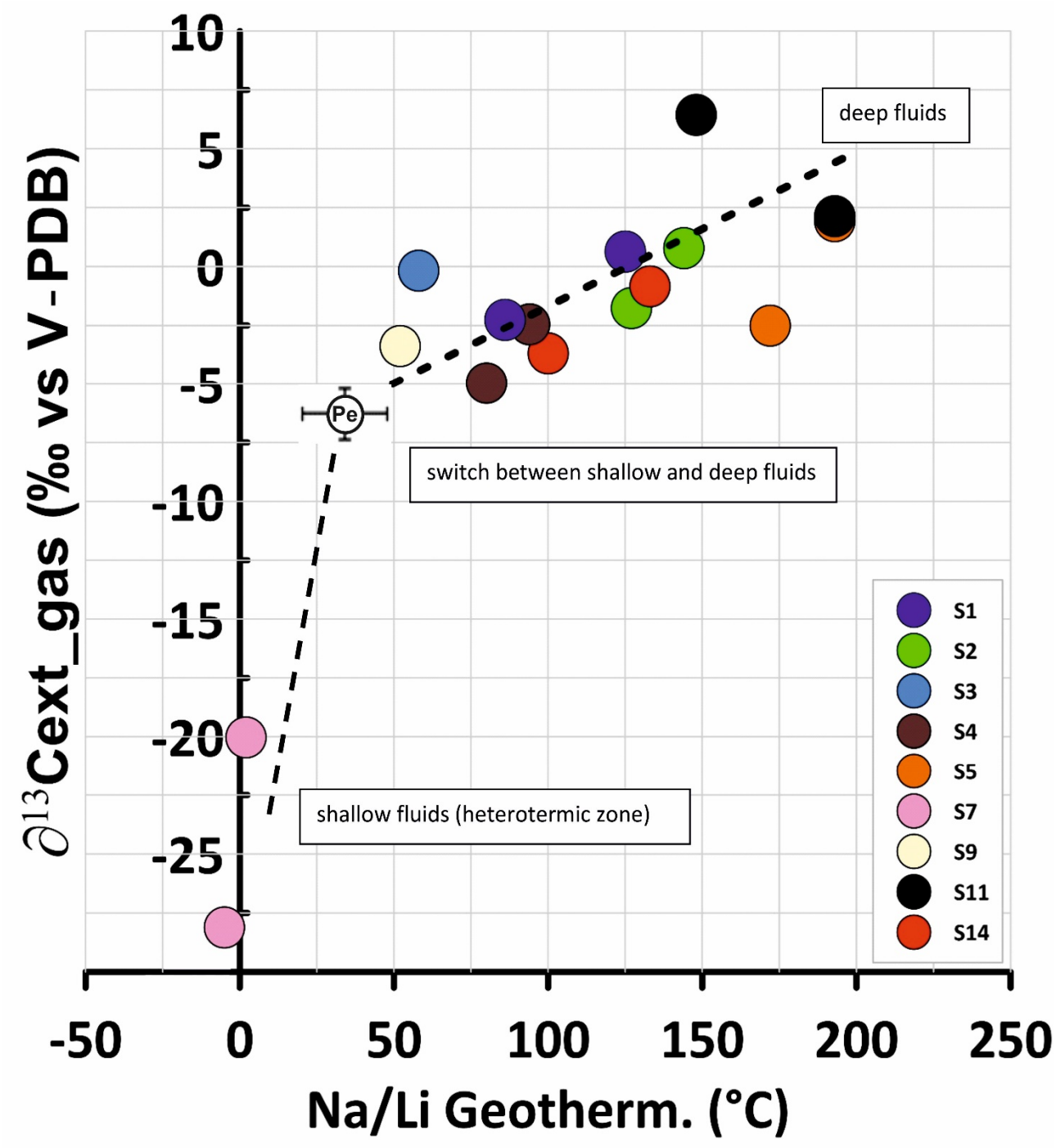

Figure 4. δ^{13}Cext versus T, where T = temperature in °C obtained from an Na-Li geothermometer [96]. δ^{13}Cext was calculated only for some groundwater samples from the San Vittorino Plain (displayed with circles), whose ($\delta^{13}C_{DIC}$) was measured. Historical data from the S10 Peschiera "Pe" spring are also shown for comparison (see also Figure S2). See Figure 1 for spring location.

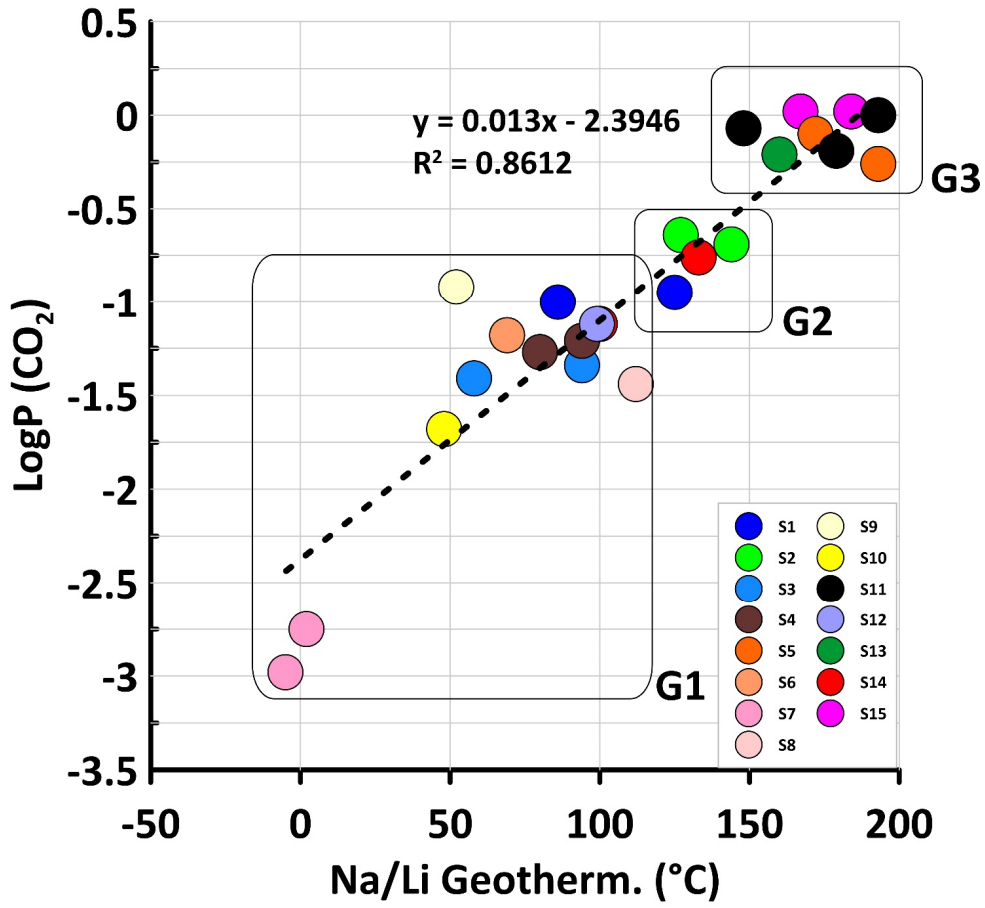

Figure 5. LogP(CO_2) at sampling conditions calculated by PHREEQCi [75] versus T, where T = temperature in °C obtained from an Na-Li geothermometer [96]. A high coefficient of determination (R-squared value = 0.86) for the groundwater samples from the San Vittorino Plain was found. See Figure 1 for spring location. G1, G2 and G3 refer to new spring groups.

Given the correlation between the temperatures inferred by the Na-Li geothermometer, the isotopic composition of CO_2 gas ($\delta^{13}C_{ext}$), logPCO_2, and some dissolved element concentrations (e.g., Li, As, Cs, and Rb), the Li-Rb-Cs ternary diagram was also developed [103] (Figure 6). Indeed, these elements generally act as less reactive and conservative elements in thermal waters, and they are often used to identify common origins or common deep processes starting from the chemical composition of waters [104,105]. Li is incorporated in secondary quartz and chlorite minerals and can be acquired directly in the dissolution process [106]. Rb and Cs are vicariants of K; therefore, they move into water solution following the leaching of minerals or alteration products rich in K (e.g., zeolites or clays). Since the Rb atomic radius is more similar to the K radius, it is a favorable vicariant with respect to Cs, which is often adsorbed on the mineral surface [107]. The analyzed groundwater covers a large area of the Li-Rb-Cs ternary diagram, as shown in Figure 6. However, three different groups of springs (G1, G2, and G3) can be clearly evidenced. The first one (G1), located close to the composition of mean limestone (the "L" field in Figure 6) [108], includes springs clearly belonging to the calcium-bicarbonate facies (S3, S4, S6, S7, S9, S10, and S12), where the water chemistry is dominated by simple interactions with the calcites and dolomites of the Mesozoic limestones (Figure 6). In central Italy, the median composition of carbonate aquifers with shallow circulation falls on the Li-Rb side of the diagram, due to a relatively low Cs concentration (0.02 ppb) [109]. Most of the Cs of the mean limestone composition is retained in low solubility impurities of the carbonate rocks. In contrast, limited enrichments in Li in some of the abovementioned springs (S3, S4, and S12) are possibly due to the mixing with groundwater circulating in the bedrock evaporitic deposits, as supported by the increase in sulphates in the same springs or eventually the uprising of

H_2S. The second group (G2) is represented by groundwater of the calcium-sulphate domain (S1, S2 and, to a lesser extent, S14; Figure 6), whose chemical compositions are attributable to a more extensive dissolution of the sulphate minerals [33,38,88]. Finally, the third group (G3) is characterized by groundwater with the highest concentrations of Li and Cs (S5, S11, S13, and S15) that suggests a different circulation model with respect to the other two groups. It is noteworthy that the samples of the second and third clusters are within or close to the ratios 1.2 < Rb/Cs < 3.0, typical of waters interacting with Upper Triassic Burano Formations [110–112], where the higher ratio is common of sulphate waters such as those from the Antrodoco area (S1, S2). In addition, the Li-Rb-Cs contents of the carbonatitic and silicate fractions of Cupaello rocks display red pentagons [41,42]. The Rb/Cs ratio seems to be similar to that of the G2 and G3 groups; however, the Li content is very different. Indeed, the Cupaello unit consists of ultrapotassic rocks, and their dissolution should give K/Na > 1, but this condition is not verified in our sampled groundwater. This fact allows to us to exclude a direct influence of magmatic rocks in the rising fluids of the San Vittorino Plain. The three groups (G1, G2, and G3) recognized through this analysis are the same as those we obtained with the geothermometric analysis (Na-Li geothermometer vs. logPCO_2 in Figure 5).

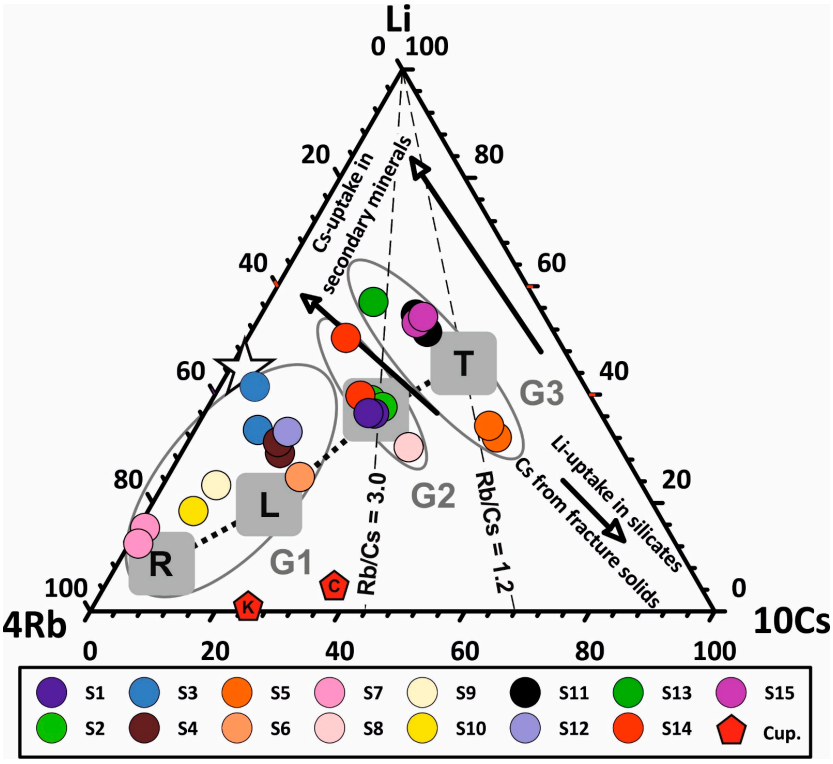

Figure 6. Li-Rb-Cs ternary diagram of the water samples (weight basis), modified after [103]. Three different groups of springs that correspond to the different steps of the water–rock interaction path (dotted line), are evidenced: (G1) groundwater of the calcium-bicarbonate water domain in the "limestone area" including S3, S4, S6, S7, S9, S10, and S12 whose water chemistry is dominated by simple interactions with calcites and dolomites of the Mesozoic limestones; that cluster contains: the "R" gray field (isochemical dissolution of mean crustal rocks) [103], the white star that depicts the median composition of carbonate aquifers with shallow circulation from central Italy [109], and the mean limestones composition "L" [108]; (G2) groundwater of the calcium-sulphate domain in the "evaporites area" including S1, S2, and S14 whose chemical compositions are attributable to a more extensive dissolution of the first groups of the sulphate minerals; and (G3) groundwater with the highest concentrations of Li and Cs including S5, S11, S13, and S15, whose geochemistry suggests a deep-seated circulation with respect to the first two groups. However, groups 2 and 3 are enclosed between 1.2 < Rb/Cs < 3.0, typical of thermal waters interacting with the Upper Triassic Burano Formations ("T" = Tuscany thermal waters [110]). The Li-Rb-Cs contents of the carbonatitic (C) and silicate (K) fractions of Cupaello rocks are shown with red pentagons (Cup.) [41,42]. See Figure 1 for spring location.

Despite this evidence of deep circulation and mixing between shallow and deep groundwater, the water stable isotopes measured only for some springs of the San Vittorino Plain (S1, S2, S4, S5, S7, S8, S10, S11, S14, and S15) did not record any significant fractionation due to upwelling of deep fluids. Indeed, the oxygen and hydrogen stable isotope compositions of central Italy's groundwater could be compared with the meteoric water lines available in the literature. Among these, the global and Mediterranean meteoric water lines, with an excess of deuterium equal to d = 10 (GMWL) [113] and d = 22 (MMWL), respectively, are the most commonly used [38,114–116]. However, it should be made clear that the value of d = 22 was inferred for the eastern Mediterranean area [117], which has very different climatic conditions from those of this study. Specifically, for central Italy, and in particular for the Latium region, the monitored meteorological events were included between water lines with a deuterium excess of between d = 12 and d = 17 [118,119]. Moreover, the central Italy meteoric water line (CIMWL) [120] and the central Italian limestone aquifer water line (LAWL) [121] are within the ribbon and have extreme lines of d = 12 and d = 17 (Figure 7). Therefore, the deuterium excess range of 12 < d < 17 could be comparable with the so-called "uncertainty wings" of meteoric waters in this area [122].

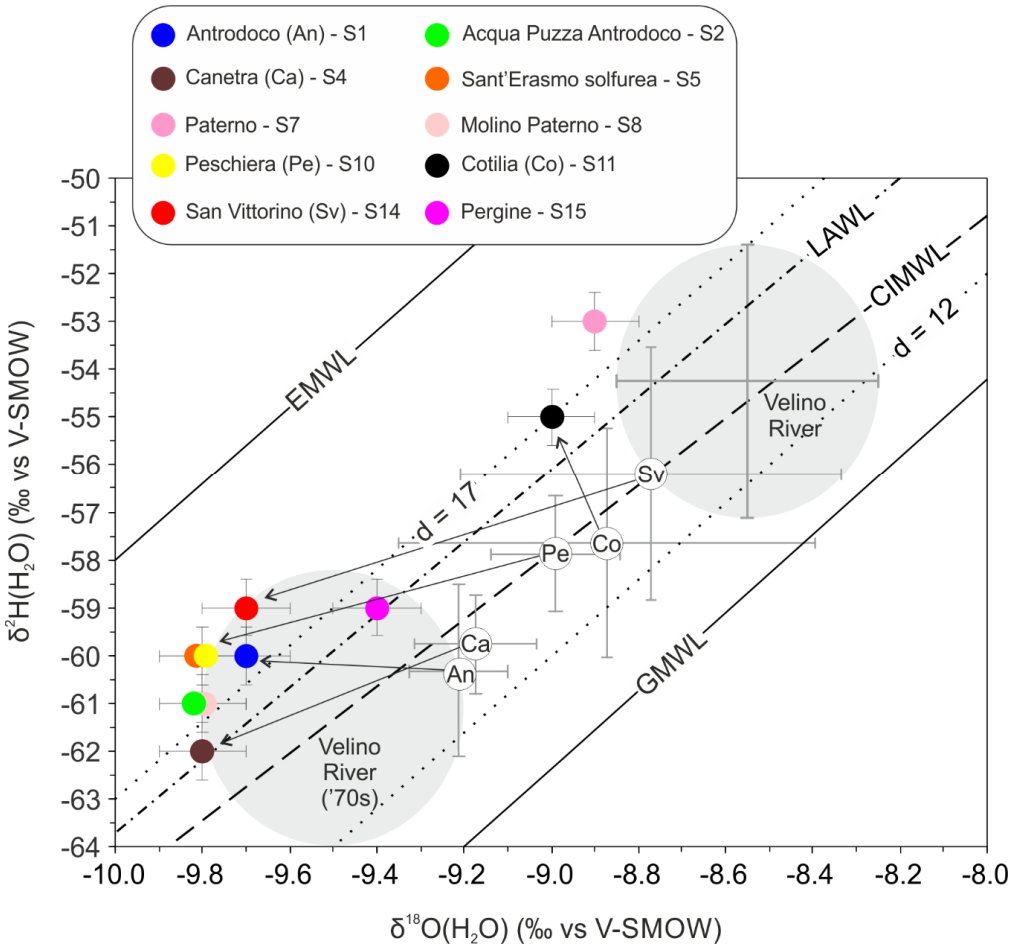

Figure 7. δ^2H-δ^{18}O (H_2O) isotope values of some samples from the San Vittorino Plain. The global and Mediterranean meteoric water lines, with excess deuterium equal to d = 10 (GMWL) [113] and d = 22 (MMWL), respectively, are used. The central Italy meteoric water line (CIMWL) [120] and the central Italy limestone aquifer water line (LAWL) [121] are also displayed within the ribbon with extreme lines of d = 12 and d = 17. Historical analyses of the isotope composition of the Velino River fall within the deuterium excess variation range of the water lines. Similarly, the groundwater of the San Vittorino Plain also falls within the compositional variation range of local rainwater. The white circles with the abbreviations Ca, An, Pe, Co, and Sv are historical data of springs with the largest standard deviation variations on historical data. See Figure 1 for spring location.

Indeed, the historical analyses of the isotope compositions of the Velino River, although showing rather significant variations over time from $\delta^{18}O = -9.5 \pm 0.3‰$ (N = 12) during the seventies [123] and $\delta^{18}O = -8.6 \pm 0.3‰$ (N = 4) in recent times [116], fall within the deuterium excess variation range of the water lines (Figure 7). Similarly, the groundwater of the San Vittorino Plain also falls within the compositional variation range of local rainwater. Figure 7 also highlights the different local recharge areas for S7 and S11, which show less negative isotopic values, indicating the lower altitude of the recharge area. All other springs show more negative isotopic values corresponding to different and higher altitudes of the recharge area, including the possible contribution of snow melting (mean $\delta^{18}O = -11‰$) [114], which was probably more significant during past meteoric recharge periods. This hypothesis is supported by the shift with time of the mean isotopic composition of surface waters, such as the Velino River (Figure 7), which shows increased isotopic values (approximately +1‰ for $\delta^{18}O$). Obviously, this shift with time is not due to a change in recharge area; consequently, this increase is due to a minor influence of high elevation areas on aquifer recharge, which can be attributed to a lower persistence of snow coverage during recent years, in line with regional climatic studies [124]. Hence, the water isotopes confirm that S7 is fed by shallow and fast-flow meteoric events infiltrating Mt. Paterno (Reatini Mts). Therefore, it represents the "shallow" end-member of our study area, comparable with the modern composition of the Velino River water (Figure 7). A similar origin can be attributed to the meteoric contribution to the S11 discharge. It should also be noted that historical analyses of some springs (e.g., S11) show considerable standard deviations both as oxygen (± 0.6‰) and as hydrogen (± 3‰) ratios (Figure 7). This significant standard deviation for S11 is probably related to the bubbling and high pressure of the dissolved gases that could enhance the evaporation effect and the variability over time of the isotopic composition of the water at the sampling site. Finally, neither ^{18}O-depletion nor ^{18}O-enrichment, due to a dominant role of CO_2 exchange with water or a significant contribution of high-temperature magmatic fluids, are distinguishable, respectively.

Differently, the analyses of free and dissolved gases in the groundwater of the San Vittorino Plain highlighted the presence of components of some volatiles different from those that are atmosphere-sourced (CO_2, CH_4, and He). In detail, He is a good tracer for recognizing the outgassing of deep-derived (mantle or crust) volatiles in continental regions, even where evidence of volcanic activity is lacking [11,125–127] because He is mainly sourced by the mantle, crust, and atmosphere, and the isotopic signatures of these three end-member reservoirs are strongly different ($^3He/^4He = 1.4 \times 10^{-6}$ in air; $\approx 10^{-5}$ mantle; $\approx 10^{-8}$ crust). In this work, the percentages of mantle-derived He and crustal He (produced by U and Th decay in the crust) were evaluated by using the approach proposed by [128], which is based on both He isotope ratios and $^4He/^{20}Ne$ ratios. Here, we assumed convective upper mantle MORB-Type (Mid Oceanic Ridge Basalts, 8 Ra) for the mantle end-member, He isotopic ratios of 0.01–0.03 Ra for the crust end member, and the atmospheric He isotope signature (1 Ra). The $^4He/^{20}Ne$ ratios of the same end-members are >1000 for the mantle and the crust and 0.318 for the atmosphere. Mainly, the reliably considered results are characterized by $^4He/^{20}Ne$ ratios higher than 10, as they do not suffer from relevant He air contamination. The samples of the San Vittorino Plain have very low contributions of mantle-derived He, which is no higher than ~1–2% (Figure 8). However, the mantle below Italy is contaminated by subduction processes, decreasing the pristine signature of the He isotopic ratio [129]. Hence, if we assume a He isotopic signature lower than the typical MORB value (8 ± 1 Ra), the mantle contribution would be higher than the above estimated values. Considering the existence of the local tectonic discontinuities that were able to drive magma batches towards the surface [130], (Figure 1), the San Vittorino graben can still act as an efficient structure that allows bottom-up interconnections for the transfer of deep-sourced volatiles to stratified regional aquifers. However, we cannot determine whether He is sourced by shallow reservoirs of mantle He stored in crustal layers [131] or directly by mantle ([73] and references therein).

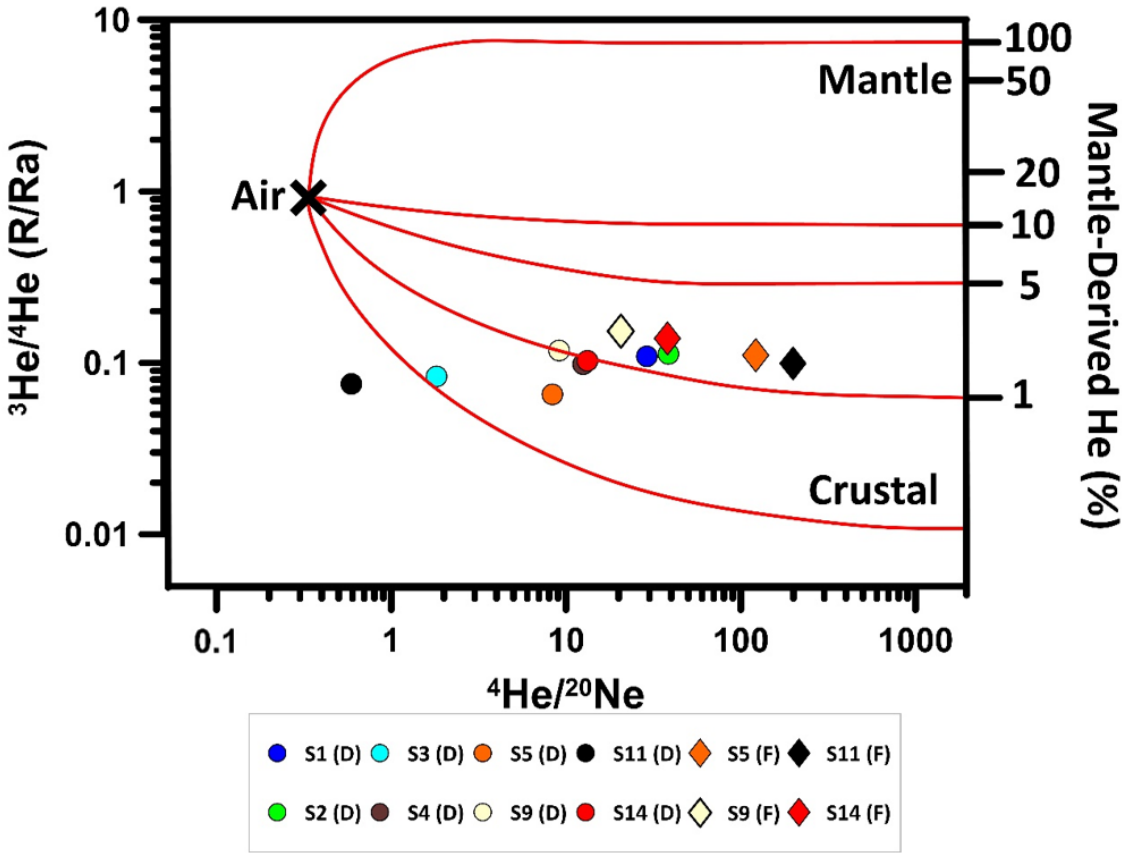

Figure 8. Diagram of ^{3}He/^{4}He (R/Ra) versus ^{4}He/^{20}Ne ratios. Mixing lines between the atmosphere and upper mantle, and the atmosphere and crust were calculated using the end members: air (^{3}He/^{4}He = 1.4 × 10^{-6}, ^{4}He/^{20}Ne = 0.318) [86], upper mantle (^{3}He/^{4}He = 12 × 10^{-6}, ^{4}He/^{20}Ne = 100,000) [132], and old continental crust (^{3}He/^{4}He = 0.02 × 10^{-6}, ^{4}He/^{20}Ne = 100,000) [131]. Samples of dissolved and free gases are named (D) and (F), respectively. See Figure 1 for spring location.

Overall, the mixing of prevailing crustal components with mantle-derived volatiles at the regional scale has also been evidenced by previous studies [11,13,20,31,32,36,65] based on He isotopes and the δ^{13}C of CO_2. This isotopic ratio can be ascribed to different sources: limestone (δ^{13}C = 0‰), organic matter (δ^{13}C = −30‰), or mantle (δ^{13}C = −6.5‰) [133]. Most of the sampled groundwater exhibits $\delta^{13}C_{ext}$ values between −5‰ and +5 ‰, which are near the values proper of the deep fluid contribution ($\delta^{13}C_{ext} = \delta^{13}C_{deep}$ = −0.35‰; Figure S2), which is different from spring S7, which shows a mean value of approximately −25‰ and is confirmed to be represented only by "infiltrating waters" ($\delta^{13}C_{inf}$) (Figure S2). Concerning the more negative values of the deep source CO_2, while $\delta^{13}C_{ext}$ values near −6‰ might result from the simple infiltration of magmatic carbon, they do not prove the existence of a mantle-derived fluid [134]. In contrast, according to [31,36], the highest/positive calculated $\delta^{13}C_{ext}$ is due to a fractionation effect related to degassing, which in the study area could reach values close to +8‰ (Figure S2). The effect of diffuse CO_2 degassing in the study area is also detectable in the Peschiera spring, where $\delta^{13}C_{ext}$ and the alkali/alkaline earth metal ratio showed concomitant variations (Figures S3 and S4). The highest value of $\delta^{13}C_{ext}$ = −4.7‰, corresponding to $\delta^{13}C_{deep}$ = +8.8‰ [36], was calculated on a sample collected just a day after the main shock occurred in Norcia (30 October 2016, magnitude moment M_w = 6.5; Figures S3 and S4 show the recalculated data of the Pe spring from [90]).

In summary, the groundwater in the San Vittorino Plain derives from complex geochemical balances that are established between water, rock, and gas. Each component of this ternary system substantially and differently affects the final geochemistry of the

groundwater, depending on the concentration of rising gases, the lithology of the aquifer, and the chemical-physical characteristics of the infiltrating water. No contributions of surface runoff to groundwater hydrogeochemistry were detected. The elaborations concerning geothermometers (Figure 5 and Supplementary File Table S1), trace elements (Figure 6 and Supplementary File Table S1), and gases (Figure 8 and Supplementary File Table S1) converge in attributing the highest temperatures (>150 °C), the greatest enrichments in Li and Cs, and traces of mantle-derived He (1–2%) to S5, S11, S13, and S15. These springs are located in peculiar sites within the San Vittorino Plain. Indeed, the waters of S11, S13, and S15 flow precisely in correspondence with the main and deeper structural elements in the area (i.e., the Fiamignano Fault and its conjugate structures; see Figures 1 and 3BB'). In addition, the water of S5 is fed by a flow influenced by the uprising of deep fluids along one of the main normal faults (orange arrow in Figure 3AA'). This observation is also corroborated by the depths inferred by geothermometric analyses that are in line with those identified in the cross-section construction. The Cs (S5) and Li (S11, S13, and S15) enrichments (or Li and Cs impoverishments, respectively) shown in Figure 6 are often related to deep processes involving silicates (clays, zeolites, quartz, or chalcedony) that often produce temperature-dependent distributions of these elements [103,135,136]. In the same area of this study, Cs enrichment up to 6.5 ppb was also detected in the "Paulla Bassa" and "Paulla 3" springs [89], which are brackish and reduced (sulphurous), similar to S5. Such a relatively high Cs concentration in old, deep-seated, and saline groundwater could also be ascribed to the long-term weathering of micaceous minerals, typically enriched in Cs, in fracture coatings and wall rock [137]. In addition, the presence of deep sourced He and CO_2 found in the same springs confirms the detailed influence of a deep circulation system, largely hidden by the huge contribution to the discharge of the shallow carbonate circulation system (as highlighted by the stability of the water isotopes). In our interpretation, the pressurized nappes can be connected via high-angle transtensive faults, which represent a preferred bottom-up connection path. The remaining two groups of springs (G1 and G2) show a degree of "deep contribution", gradually decreasing with respect to the deep fluids uprising. These springs are located at the intersection with secondary structural elements that are probably not able to allow a relevant uprising of deep fluids. In some cases (e.g., S10), the great abundance of shallow waters may hinder the deep signal.

Although this area is characterized by intense degassing and evident chemical and isotopic features of mixing of shallow and deep fluids, there are only some springs whose hydrogeochemical features are directly connected with deep structures. In detail, their depth corresponds to the common hypocenters of earthquakes in the Apennine chain (7–10 km) because of the direct connection of the tectonic lines allowing the upward migration of fluids along high-angle faults. Furthermore, the springs of potential interest are those least affected by shallow circulation (also in terms of seasonal variations). For future research, the investigations should be based on high-frequency multiparametric monitoring at different sites and on data cross analysis, through which the dynamics and time evolution of processes in relation to the seismicity of the central Apennines region could be characterized in more detail [100].

In addition, for the management and exploitation of water resources, sites such as the San Vittorino Plain require careful monitoring of the huge quantities of available high-quality water resources, as they could undergo alterations in their chemical-physical properties induced by uprising deep fluids rich in CO_2 and heavy metals. For example, the groundwaters of S5, S11, S13, and S15 show concentrations of As between 4 and 60 ppb, probably owing to the greater amount of dissolved CO_2. These factors can become relevant for future scenarios of climate change, which can increase heavy metal concentrations. Similarly, the large quantities of dissolved CO_2 make the waters more aggressive towards calcium carbonate, increasing the already high sinkhole risk in the area [68].

6. Conclusions

The San Vittorino Plain, an intramontane plain where a large amount of groundwater resources converges from large mountain fractured aquifers to several springs affected by different degrees of mineralization, represents one of the more interesting areas for evaluating groundwater mixing of direct rainfall recharge components with deep fluids uprising along high-angle faults reaching a depth of at least 5 km b.s.l. In our study, we suggest a methodological approach useful for improving groundwater monitoring aimed at identifying geochemical signals related to crustal deformation and potentially to seismic activity.

Analysis of the results of major and trace elements, stable isotopes of water, chemistry and isotopes of dissolved and free gases, coupled with an updated geo-structural setting and very detailed knowledge of the hydrogeology, allowed us to build a robust conceptual model where all elements converge into a coherent framework. By applying different geothermometers, a reliable thermodynamic balance reveals the Na-Li geothermometer as an affordable tool for calculating the equilibrium temperature of the deep contributions, established at approximately 150–200 °C. Such deep fluids show a hydrogen and oxygen isotope composition typical of meteoric water, whereas the ^{18}O-enriched component typical of high-temperature magmatic fluids is substantially absent. However, the analysis of He and CO_2 isotopes confirms the presence of a deep component with possible traces of mantle-derived helium (1–2%). Trace element occurrence clarifies the water–rock interaction processes and supports the conceptual model based on the localized uprising of deep fluids that do not casually match the distribution of high-angle faults that are capable of connecting different reservoirs delimited by less permeable thrust zones. The distribution and concentration of deep fluids uprising and spreading into the aquifers cause significant changes in the classical calcium-bicarbonate equilibrium of the basal springs, allowing the subdivision of the sampled selected springs into three groups showing different degrees of deep contribution (G1, G2, and G3).

On the basis of the reviewed structural map, the geological setting shown in the cross-sections presented herein could also make possible the uprising of deep-derived gases in the Velino Valley. In this sketched model, it is now clear that these high-angle faults work as a network of pathways through which deep fluids reach the shallow regional aquifers that are otherwise totally recharged by meteoric infiltration. Based on geothermometrical analysis and structural cross sections, we inferred the origin of the deep fluid portion at a depth of approximately 7–10 km, where Apennine earthquakes usually occur. Consequently, this integrated approach can help identify the most suitable sites aimed at analyzing the relationships between groundwater and seismicity. Indeed, knowing the mixing degree among different springs, it is possible to recognize whether and where the flux of the deep portion, modulated by fault activity, increases or decreases with respect to permeability variations along the uprising zones.

A list of possible criteria found within this study for the optimization of future groundwater hydrogeochemical monitoring aimed at correlating crustal deformation along faults and related (micro- and perhaps macro-) seismicity can be summarized as follows: (a) discharge areas with concentrations of different hydrochemical spring characteristics; (b) steady base flow from regional aquifers recharged by meteoric infiltration; (c) selection of the most representative sampling sites on the basis of a complete hydrochemical/isotopic analysis; and (d) review of fault geometries at the surface and depth. We consider the future possible establishment of a groundwater monitoring network based on the abovementioned criteria to be very useful for improving the contribution of groundwater monitoring to the wide research field of earthquake precursors.

Supplementary Materials: The following are available online at https://www.mdpi.com/2076-3417/11/4/1353/s1: Table S1: Chemical data; Figure S1: Detail of Langelier–Ludwig diagram; Figure S2: δ^{13}Cext versus 1/Cext diagram; Figure S3: Time series of the Y-coordinate of the Langelier–

Ludwig diagram and δ^{13}Cext parameter at Peschiera spring (Pe); Figure S4: Moving averages on Figure S3 data

Author Contributions: Conceptualization, M.D.B., M.P., A.C.; Data curation, M.D.B.; F.G. T.B., G.L.C.; Formal analysis, M.D.B., F.G., M.P.; Investigation, M.D.B., M.P., A.C.; Methodology, M.D.B., F.G., M.B., G.L.C.; Project administration, M.P.; Resources, M.B., A.C., M.P.; Supervision, M.P., M.B., T.B.; Validation, M.P., T.B., M.B.; Writing—original draft, M.D.B., F.G., T.B., G.L.C.; Writing—review & editing, M.P., T.B, A.C. M.B.; Geological and Hydrogeological framing G.L.C. All authors reviewed the manuscript and figures and approved their submission to Applied Sciences. All authors have read and agreed to the published version of the manuscript.

Funding: This research received no external funding.

Institutional Review Board Statement: Not applicable.

Informed Consent Statement: Not applicable.

Data Availability Statement: The data presented in this study are openly available in Supplementary Files.

Acknowledgments: All the staff of the Laboratorio di Idrogeologia Quantitativa (Sapienza University of Rome) are thanked for their logistic and technical support. We thank Giulia Esposito for the preliminary results obtained in the Master's degree thesis focused on this study site. We also thank INGV-Palermo for supporting the analysis carried out in its laboratories and Mariano Tantillo, Ygor Oliveri, and Francesco Salerno for their analytical contribution. Thanks is also given to the anonymous reviewers who provided very useful comments which significantly improved the original manuscript.

Conflicts of Interest: The authors declare no conflict of interest.

References

1. Edmunds, W.M.; Smedley, P.L. Residence time indicators in groundwater: The East Midlands Triassic sandstone aquifer. *Appl. Geochem.* **2000**, *15*, 737–752. [CrossRef]
2. Goldscheider, N.; Mádl-Szőnyi, J.; Erőss, A.; Schill, E. Review: Thermal water resources in carbonate rock aquifers. *Hydrogeol. J.* **2010**, *18*, 1303–1318. [CrossRef]
3. Skelton, A.; Liljedahl-Claesson, L.; Wästeby, N.; Andrén, M.; Stockmann, G.; Sturkell, E.; Mörth, C.M.; Stefansson, A.; Tollefsen, E.; Siegmund, H.; et al. Hydrochemical Changes Before and After Earthquakes Based on Long-Term Measurements of Multiple Parameters at Two Sites in Northern Iceland—A Review. *J. Geophys. Res. Solid Earth* **2019**, *124*, 2702–2720. [CrossRef]
4. Singh, P.; Mukherjee, S. Chemical signature detection of groundwater and geothermal waters for evidence of crustal deformation along fault zones. *J. Hydrol.* **2020**, *582*, 124459. [CrossRef]
5. Cardello, G.L.; Mancktelow, N.S. Veining and post-nappe transtensional faulting in the SW Helvetic Alps (Switzerland). *Swiss J. Geosci.* **2015**, *108*, 379–400. [CrossRef]
6. Clemenzi, L.; Storti, F.; Balsamo, F.; Molli, G.; Ellam, R.; Muchez, P.; Swennen, R. Fluid pressure cycles, variations in permeability, and weakening mechanisms along low-angle normal faults: The Tellaro detachment, Italy. *Geol. Soc. Am. Bull.* **2015**, *127*, 1689–1710. [CrossRef]
7. Agosta, F.; Kirschner, D.L. Fluid conduits in carbonate-hosted seismogenic normal faults of central Italy: Fluid conduits in seismogenic normal faults. *J. Geophys. Res.* **2003**, *108*. [CrossRef]
8. Cardello, G.L. The Rawil Depression: Its Structural History from Cretaceous to Neogene. Ph.D. Thesis, ETH Zurich, Zürich, Switzerland, 2013; p. 1 Band.
9. Smeraglia, L.; Aldega, L.; Bernasconi, S.M.; Billi, A.; Boschi, C.; Caracausi, A.; Carminati, E.; Franchini, S.; Rizzo, A.L.; Rossetti, F.; et al. The role of trapped fluids during the development and deformation of a carbonate/shale intra-wedge tectonic mélange (Mt. Massico, Southern Apennines, Italy). *J. Struct. Geol.* **2020**, *138*, 104086. [CrossRef]
10. Miller, S.A.; Nur, A. Permeability as a toggle switch in fluid-controlled crustal processes. *Earth Planet. Sci. Lett.* **2000**, *183*, 133–146. [CrossRef]
11. Italiano, F.; Martelli, M.; Martinelli, G.; Nuccio, P.M. Geochemical evidence of melt intrusions along lithospheric faults of the Southern Apennines, Italy: Geodynamic and seismogenic implications. *J. Geophys. Res.* **2001**, *105*, 13569–13578. [CrossRef]
12. Chiodini, G.; Cardellini, C.; Amato, A.; Boschi, E.; Caliro, S.; Frondini, F.; Ventura, G. Carbon dioxide Earth degassing and seismogenesis in central and southern Italy: Carbon dioxide earth degassing and seismogenesis. *Geophys. Res. Lett.* **2004**, *31*. [CrossRef]
13. Italiano, F.; Bonfanti, P.; Ditta, M.; Petrini, R.; Slejko, F. Helium and carbon isotopes in the dissolved gases of Friuli Region (NE Italy): Geochemical evidence of CO_2 production and degassing over a seismically active area. *Chem. Geol.* **2009**, *266*, 76–85. [CrossRef]
14. Doglioni, C.; Barba, S.; Carminati, E.; Riguzzi, F. Fault on–off versus coseismic fluids reaction. *Geosci. Front.* **2014**, *5*, 767–780. [CrossRef]

15. Smeraglia, L.; Bernasconi, S.M.; Berra, F.; Billi, A.; Boschi, C.; Caracausi, A.; Carminati, E.; Castorina, F.; Doglioni, C.; Italiano, F.; et al. Crustal-scale fluid circulation and co-seismic shallow comb-veining along the longest normal fault of the central Apennines, Italy. *Earth Planet. Sci. Lett.* **2018**, *498*, 152–168. [CrossRef]
16. Collettini, C.; Tesei, T.; Scuderi, M.M.; Carpenter, B.M.; Viti, C. Beyond Byerlee friction, weak faults and implications for slip behavior. Earth Planet. *Sci. Lett.* **2019**, *519*, 245–263. [CrossRef]
17. Buttitta, D.; Caracausi, A.; Chiaraluce, L.; Favara, R.; Gasparro, M.; Sulli, A. Evidences of the role of seismicity on degassing of volatile through the crust. *Sci. Rep.* **2020**, *10*, 1–13. [CrossRef]
18. Italiano, F.; Solecki, A.; Martinelli, G.; Wang, Y.; Zheng, G. New Applications in Gas Geochemistry. *Geofluids* **2020**, *2020*, 1–3. [CrossRef]
19. Caracausi, A.; Italiano, F.; Martinelli, G.; Paonita, A.; Rizzo, A. Long-term geochemical monitoring and extensive/compressive phenomena: Case study of the Umbria Region (Central Apennines, Italy). *Ann. Geophys.* **2005**, *48*, 43–53.
20. Italiano, F.; Caracausi, A.; Favara, R.; Innocenzi, P.; Martinelli, G. Geochemical monitoring of cold waters during seismicity: Implications for earthquake-induced modification in shallow aquifers. *Terr. Atmos. Ocean. Sci.* **2005**, *16*, 709. [CrossRef]
21. Barberio, M.D.; Barbieri, M.; Billi, A.; Doglioni, C.; Petitta, M. Hydrogeochemical changes before and during the 2016 Amatrice-Norcia seismic sequence (central Italy). *Sci. Rep.* **2017**, *7*, 11735. [CrossRef]
22. Boschetti, T.; Barbieri, M.; Barberio, M.D.; Billi, A.; Franchini, S.; Petitta, M. CO_2 Inflow and Elements Desorption Prior to a Seismic Sequence, Amatrice-Norcia 2016, Italy. *Geochem. Geophys. Geosyst.* **2019**, *20*, 2303–2317. [CrossRef]
23. Cappa, F.; Scuderi, M.M.; Collettini, C.; Guglielmi, Y.; Avouac, J.-P. Stabilization of fault slip by fluid injection in the laboratory and in situ. *Sci. Adv.* **2019**, *5*, eaau4065. [CrossRef]
24. Hosono, T.; Masaki, Y. Post-seismic hydrochemical changes in regional groundwater flow systems in response to the 2016 Mw 7.0 Kumamoto earthquake. *J. Hydrol.* **2020**, *580*, 124340. [CrossRef]
25. Shi, Z.; Zhang, H.; Wang, G. Groundwater trace elements change induced by M5.0 earthquake in Yunnan. *J. Hydrol.* **2020**, *581*, 124424. [CrossRef]
26. Hartmann, J.; Levy, J.K. Hydrogeological and Gasgeochemical Earthquake Precursors? A Review for Application. *Nat. Hazards* **2005**, *34*, 279–304. [CrossRef]
27. Uysal, I.T.; Feng, Y.; Zhao, J.; Isik, V.; Nuriel, P.; Golding, S.D. Hydrothermal CO_2 degassing in seismically active zones during the late Quaternary. *Chem. Geol.* **2009**, *265*, 442–454. [CrossRef]
28. Tesei, T.; Collettini, C.; Barchi, M.R.; Carpenter, B.M.; Di Stefano, G. Heterogeneous strength and fault zone complexity of carbonate-bearing thrusts with possible implications for seismicity. *Earth Planet. Sci. Lett.* **2014**, *408*, 307–318. [CrossRef]
29. Scuderi, M.M.; Collettini, C. The role of fluid pressure in induced vs. triggered seismicity: Insights from rock deformation experiments on carbonates. *Sci. Rep.* **2016**, *6*, 24852. [CrossRef]
30. Italiano, F.; Martinelli, G.; Plescia, P. CO_2 Degassing over Seismic Areas: The Role of Mechanochemical Production at the Study Case of Central Apennines. *Pure Appl. Geophys.* **2008**, *165*, 75–94. [CrossRef]
31. Giustini, F.; Blessing, M.; Brilli, M.; Lombardi, S.; Voltattorni, N.; Widory, D. Determining the origin of carbon dioxide and methane in the gaseous emissions of the San Vittorino plain (Central Italy) by means of stable isotopes and noble gas analysis. *Appl. Geochem.* **2013**, *34*, 90–101. [CrossRef]
32. Caracausi, A.; Paternoster, M. Radiogenic helium degassing and rock fracturing: A case study of the southern Apennines active tectonic region. *J. Geophys. Res. Solid Earth* **2015**, *120*, 2200–2211. [CrossRef]
33. Barbieri, M.; Boschetti, T.; Barberio, M.D.; Billi, A.; Franchini, S.; Iacumin, P.; Selmo, E.; Petitta, M. Tracing deep fluid source contribution to groundwater in an active seismic area (central Italy): A combined geothermometric and isotopic (δ13C) perspective. *J. Hydrol.* **2020**, *582*, 124495. [CrossRef]
34. Carminati, E.; Doglioni, C. Alps vs. Apennines: The paradigm of a tectonically asymmetric Earth. *Earth Sci. Rev.* **2012**, *112*, 67–96. [CrossRef]
35. Boni, C.; Bono, P.; Capelli, G. Schema Idrogeologico Dell'Italia Centrale. *Mem. Soc. Geol.* **1986**, *35*, 991–1012.
36. Chiodini, G.; Cardellini, C.; Di Luccio, F.; Selva, J.; Frondini, F.; Caliro, S.; Rosiello, A.; Beddini, G.; Ventura, G. Correlation between tectonic CO_2 Earth degassing and seismicity is revealed by a 10-year record in the Apennines, Italy. *Sci. Adv.* **2020**, *6*, eabc2938. [CrossRef]
37. Madonia, P.; Cangemi, M.; Oliveri, Y.; Germani, C. Hydrogeochemical Characters of Karst Aquifers in Central Italy and Relationship with Neotectonics. *Water* **2020**, *12*, 1926. [CrossRef]
38. Petitta, M.; Primavera, P.; Tuccimei, P.; Aravena, R. Interaction between deep and shallow groundwater systems in areas affected by Quaternary tectonics (Central Italy): A geochemical and isotope approach. *Environ. Earth Sci.* **2011**, *63*, 11–30. [CrossRef]
39. Petitta, M. Idrogeologia della media valle del fiume velino e della piana di s. Vittorino (Rieti, Italia centrale) / hydrogeology of the middle valley of the velino river and of the s. Vittorino plain (Rieti, Central Italy). *Ital. J. Eng. Geol. Environ.* **2009**, 157–181. [CrossRef]
40. Centamore, E.; Nisio, S.; Rossi, D. The San Vittorino Sinkhole Plain: Relationships between bedrock structure, sinking processes, seismic events and hydrothermal springs. *Ital. J. Geosci.* **2009**, *128*, 629–639.
41. Stoppa, F.; Cundari, A. A new Italian carbonatite occurrence at Cupaello (Rieti) and its genetic significance. *Contrib. Mineral. Petrol.* **1995**, *122*, 275–288. [CrossRef]

42. Peccerillo, A. *Plio-Quaternary Volcanism in Italy*; Springer: Berlin/Heidelberg, Germany; New York, NY, USA, 2005; Volume 365, ISBN 978-3-540-25885-8.
43. Barbieri, M. Groundwater mixing in the discharge area of San Vittorino Plain (Central Italy): Geochemical characterization and implication for drinking uses. *Environ. Earth. Sci.* **2017**, *76*, 393. [CrossRef]
44. Doglioni, C. A proposal for the kinematic modelling of W-dipping subductions—possible applications to the Tyrrhenian-Apennines system. *Terra Nova* **1991**, *3*, 423–434. [CrossRef]
45. Patacca, E.; Scandone, P. Geology of the southern Apennines. *Boll. Della Soc. Geol. Ital.* **2007**, *7*, 75–119.
46. Carminati, E.; Fabbi, S.; Santantonio, M. Slab bending, syn-subduction normal faulting, and out-of-sequence thrusting in the Central Apennines: Effects of slab bending in the Apennines. *Tectonics* **2014**, *33*, 530–551. [CrossRef]
47. Centamore, E.; Nisio, S. Tettonica e sedimentazione (Lias-Pleistocene) nella media Valle del Salto (Rieti, Italia Centrale). *Stud. Geol. Camerti* **2002**, *2*, 53–70.
48. Cardello, G.L.; Doglioni, C. From Mesozoic rifting to Apennine orogeny: The Gran Sasso range (Italy). *Gondwana Res.* **2015**, *27*, 1307–1334. [CrossRef]
49. Bigi, S.; Costa Pisani, P. From a deformed Peri-Tethyan carbonate platform to a fold-and-thrust-belt: An example from the Central Apennines (Italy). *J. Struct. Geol.* **2005**, *27*, 523–539. [CrossRef]
50. Deiana, G.; Pasqualini, L.; Salvucci, R.; Stroppa, P.; Tondi, E. Il sistema dei sovrascorrimenti dei Monti Reatini: Analisi geometrica e cinematica. *Stud. Geol. Camerti* **1995**, 199–206.
51. Chiarabba, C.; Jovane, L.; DiStefano, R. A new view of Italian seismicity using 20 years of instrumental recordings. *Tectonophysics* **2005**, *395*, 251–268. [CrossRef]
52. D'Agostino, N. Complete seismic release of tectonic strain and earthquake recurrence in the Apennines (Italy). *Geophys. Res. Lett.* **2014**, *41*, 1155–1162. [CrossRef]
53. Cavinato, G.P.; Celles, P.D. Extensional basins in the tectonically bimodal central Apennines fold-thrust belt, Italy: Response to corner flow above a subducting slab in retrograde motion. *Geology* **1999**, *27*, 955–958. [CrossRef]
54. Centamore, E.; Nisio, S.; Rossi, D. Aspetti geologico-strutturali in relazione alla formazione della 'sinkhole plain' di S. Vittorino. In Proceedings of the State of the Art on the Study of Sinkhole Phenomena and Role of the National and Local Government in the Territory Administration, Rome, Italy, 20–21 May 2004.
55. Carrara, C.; Brunamonte, F.; Ferreli, L.; Lorenzoni, P.; Margheriti, L.; Michetti, A.M.; Raglione, M.; Rosati, M.; Serva, L. I terrazzi della medio-bassa Valle del Fiume Velino. *Stud. Geol. Camerti* **1993**, *1992*, 97–102.
56. Castellarin, A.; Colacicchi, R.; Praturlon, A.; Cantelli, C. The jurassic-lower pliocene history of the Ancona-Anzio Line (Central Italy). *Mem. Della Soc. Geol. Ital.* **1982**, *24*, 325–336.
57. Butler, R.W.H.; Tavarnelli, E.; Grasso, M. Structural inheritance in mountain belts: An Alpine–Apennine perspective. *J. Struct. Geol.* **2006**, *28*, 1893–1908. [CrossRef]
58. Pizzi, A.; Galadini, F. Pre-existing cross-structures and active fault segmentation in the northern-central Apennines (Italy). *Tectonophysics* **2009**, *476*, 304–319. [CrossRef]
59. Dramis, F. Il ruolo dei sollevamenti tettonici a largo raggio nella genesi del rilievo appenninico. *Stud. Geol. Camerti* **1993**, *1*, 9–15.
60. Faccenna, C.; Florindo, F.; Funiciello, R.; Lombardi, S. Tectonic setting and Sinkhole Features: Case histories from western Central Italy. In *Neotectonics: Recent Advances. Quaternary Proceedings*; Owen, L.A., Stewart, I., Vita-Finzi, C., Eds.; Quaternary Research Association: Cambridge, UK, 1993; Volume 3, pp. 47–56.
61. Centamore, E.; Nisio, S. Effects of uplift and tilting in the Central-Northern Apennines (Italy). *Quat. Int.* **2003**, *101–102*, 93–101. [CrossRef]
62. D'Agostino, N.; Jackson, J.A.; Dramis, F.; Funiciello, R. Interactions between mantle upwelling, drainage evolution and active normal faulting: An example from the central Apennines (Italy). *Geophys. J. Int.* **2001**, *147*, 475–497. [CrossRef]
63. Fiorillo, F.; Petitta, M.; Preziosi, E.; Rusi, S.; Esposito, L.; Tallini, M. Long-term trend and fluctuations of karst spring discharge in a Mediterranean area (central-southern Italy). *Environ. Earth Sci.* **2015**, *74*, 153–172. [CrossRef]
64. Boni, C.; Petitta, M. Sorgenti lineari e valutazione dell'infiltrazione efficace in alcuni bacini dell'Italia Centrale. *Quad. Geol. Appl.* **1994**, *1*, 99–113.
65. Chiodini, G.; Cardellini, C.; Caliro, S.; Chiarabba, C.; Frondini, F. Advective heat transport associated with regional Earth degassing in central Apennine (Italy). *Earth Planet. Sci. Lett.* **2013**, *373*, 65–74. [CrossRef]
66. Lombardi, S.; Annunziatellis, A.; Beaubien, S.E.; Ciotoli, G. Near-surface gas geochemistry techniques to assess and monitor CO2 geological sequestration sites. In *Advances in the Geological Storage of Carbon Dioxide*; Lombardi, S., Altunina, L.K., Beaubien, S.E., Eds.; Kluwer Academic Publishers: Dordrecht, The Netherlands, 2006; Volume 65, pp. 141–156. ISBN 978-1-4020-4469-4.
67. Salvati, R.; Sasowsky, I.D. Development of collapse sinkholes in areas of groundwater discharge. *J. Hydrol.* **2002**, *264*, 1–11. [CrossRef]
68. Annunziatellis, A.; Beaubien, S.E.; Ciotoli, G.; Lombardi, S.; Nisio, S.; Nolasco, F. Studio dei parametri geologici e geochimici per la comprensione dei meccanismi genetici degli sprofondamenti nella piana di S. Vittorino (Rieti). In Proceedings of the State of the Art on the Study of Sinkhole Phenomena and Role of the National and Local Government in the Territory Administration, Rome, Italy, 20–21 May 2004.

69. Bridgewater, L.L.; Baird, R.B. *Standard Methods for the Examination of Water and Wasterwater*, 23rd ed.; American Public Health Association, American Water Works Association, Water Environment Federation, Eds.; American Public Health Association: Washington, DC, USA, 2017; ISBN 978-0-87553-287-5.
70. Nigro, A.; Sappa, G.; Barbieri, M. Application of boron and tritium isotopes for tracing landfill contamination in groundwater. *J. Geochem. Explor.* **2017**, *172*, 101–108. [CrossRef]
71. Epstein, S.; Mayeda, T. Variation of O18 content of waters from natural sources. *Geochim. Cosmochim. Acta* **1953**, *4*, 213–224. [CrossRef]
72. Capasso, G.; Favara, R.; Grassa, F.; Inguaggiato, S.; Longo, L. On-line technique for preparing and measuring stable carbon isotope of total dissolved inorganic carbon in water samples (d13CTDIC). *Ann. Geophys.* **2005**, *48*, 159–166.
73. Caracausi, A.; Sulli, A. Outgassing of Mantle Volatiles in Compressional Tectonic Regime Away From Volcanism: The Role of Continental Delamination. *Geochem. Geophys. Geosyst.* **2019**, *20*, 2007–2020. [CrossRef]
74. Capasso, G.; Inguaggiato, S. A simple method for the determination of dissolved gases in natural waters. An application to thermal waters from Vulcano Island. *Appl. Geochem.* **1998**, *13*, 631–642. [CrossRef]
75. Parkhurst, D.L.; Appelo, C.A.J. Description of Input and Examples for PHREEQC Version 3—A Computer Program for Speciation, Batch-Reaction, One-Dimensional Transport, and Inverse Geochemical Calculations, (USGS). 2013. Available online: https://pubs.usgs.gov/tm/06/a43/ (accessed on 10 April 2020).
76. Bethke, C. *Geochemical and Biogeochemical Reaction Modeling*, 2nd ed.; Oxford University Press: Cambridge, UK; New York, NY, USA, 2008; ISBN 978-0-521-87554-7.
77. Chiodini, G.; Frondini, F.; Cardellini, C.; Parello, F.; Peruzzi, L. Rate of diffuse carbon dioxide Earth degassing estimated from carbon balance of regional aquifers: The case of central Apennine, Italy. *J. Geophys. Res.* **2000**, *105*, 8423–8434. [CrossRef]
78. Plummer, L.N.; Prestemon, E.C.; Parkhurst, D.L. An interactive code (NETPATH) for modeling net geochemical reactions along a flow path, version 2.0. *Water Resour. Investig. Rep.* **1994**, *94*, 4169.
79. Parkhurst, D.L.; Charlton, S.R. *NetpathXL—An Excel Interface to the Program NETPATH*; U.S. Geological Survey Techniques and Methods 6–A26; USGS: Reston, VA, USA, 2008.
80. Di Luccio, F.; Chiodini, G.; Caliro, S.; Cardellini, C.; Convertito, V.; Pino, N.A.; Tolomei, C.; Ventura, G. Seismic signature of active intrusions in mountain chains. *Sci. Adv.* **2018**, *4*, e1701825. [CrossRef]
81. Frondini, F.; Cardellini, C.; Caliro, S.; Beddini, G.; Rosiello, A.; Chiodini, G. Measuring and interpreting CO 2 fluxes at regional scale: The case of the Apennines, Italy. *J. Geol. Soc.* **2019**, *176*, 408–416. [CrossRef]
82. Masi, U.; Tucci, P.; Azzaro, E. Chemiostratigrafia e petrografia della formazione dolomitica triassica di Antrodoco (Rieti, Lazio settentrionale). *Geol. Romana* **1995**, *31*, 307–318.
83. OriginLab. *Origin User Guide*; OriginLab Corporation: Northampton, MA, USA, 2018.
84. Capotorti, F.; Fumanti, F.; Mariotti, G. Carta geologica del settore compreso tra il M. Nuria, il M. Gabbia e l'alta valle del F. Velino (Appennino Centrale)—scala 1: 50000. *Stud. Geol. Camerti* **1996**. Available online: http://193.204.8.201:8080/jspui/handle/1336/763 (accessed on 10 April 2020).
85. Piper, A.M. A graphic procedure in the geochemical interpretation of water-analyses. *Trans. AGU* **1944**, *25*, 914. [CrossRef]
86. Ozima, M.; Podosek, F.A. *Noble Gas Geochemistry*, 2nd ed.; Cambridge University Press: Cambridge, UK; New York, NY, USA, 2002; ISBN 978-0-521-80366-3.
87. Defennu, L.; Lombardi, S.; Federici, C. An introductory note on statistical analysis of physio-chemical characteristics of natural waters. Application to some Central Apennines spring waters. Atti della Accademia Nazionale dei Lincei. Classe di Scienze Fisiche, Matematiche e Naturali. *Rendiconti* **1975**, *59*, 125–139.
88. Governa, M.E.; Masciocco, L.; Riba, M.; Zuppi, G.M.; Lombardi, S. Karst and geothermal water circulation in the Central Apennines (Italy). In *Isotope Techniques in the Study of the Hydrology of Fractured and Fissured Rocks*; International Atomic Energy Agency: Vienna, Austria, 1989.
89. Civita, M.V.; Fiorucci, A. The recharge-discharge process of the Peschiera spring system (central Italy). *Aqua Mundi* **2010**, *1*, 161–178.
90. Rosen, M.R.; Binda, G.; Archer, C.; Pozzi, A.; Michetti, A.M.; Noble, P.J. Mechanisms of Earthquake-Induced Chemical and Fluid Transport to Carbonate Groundwater Springs After Earthquakes. *Water Resour. Res.* **2018**, *54*, 5225–5244. [CrossRef]
91. Battistel, M.; Hurwitz, S.; Evans, W.; Barbieri, M. Multicomponent Geothermometry Applied to a Medium-low Enthalpy Carbonate-evaporite Geothermal Reservoir. *Energy Procedia* **2014**, *59*, 359–365. [CrossRef]
92. Marini, L.; Chiodini, G.; Cioni, R. New geothermometers for carbonate—evaporite geothermal reservoirs. *Geothermics* **1986**, *15*, 77–86. [CrossRef]
93. Minissale, A.A.; Duchi, V. Geothermometry on fluids circulating in a carbonate reservoir in north-central Italy. *J. Volcanol. Geotherm. Res.* **1988**, *35*, 237–252. [CrossRef]
94. Chiodini, G.; Cioni, R.; Guidi, M.; Marini, L. Chemical geothermometry and geobarometry in hydrothermal aqueous solutions: A theoretical investigation based on a mineral-solution equilibrium model. *Geochim. Cosmochim. Acta* **1991**, *55*, 2709–2727. [CrossRef]
95. Chiodini, G.; Frondini, F.; Marini, L. Theoretical geothermometers and PCO2 indicators for aqueous solutions coming from hydrothermal systems of medium-low temperature hosted in carbonate-evaporite rocks. Application to the thermal springs of the Etruscan Swell, Italy. *Appl. Geochem.* **1995**, *10*, 337–346. [CrossRef]

96. Sanjuan, B.; Millot, R.; Ásmundsson, R.; Brach, M.; Giroud, N. Use of two new Na/Li geothermometric relationships for geothermal fluids in volcanic environments. *Chem. Geol.* **2014**, *389*, 60–81. [CrossRef]
97. Ford, D.; Williams, P.W. *Karst Hydrogeology and Geomorphology*; John Wiley & Sons: Chichester, UK; Hoboken, NJ, USA, 2007; ISBN 978-0-470-84996-5.
98. Awaleh, M.O.; Boschetti, T.; Adaneh, A.E.; Daoud, M.A.; Ahmed, M.M.; Dabar, O.A.; Soubaneh, Y.D.; Kawalieh, A.D.; Kadieh, I.H. Hydrochemistry and multi-isotope study of the waters from Hanlé-Gaggadé grabens (Republic of Djibouti, East African Rift System): A low-enthalpy geothermal resource from a transboundary aquifer. *Geothermics* **2020**, *86*, 101805. [CrossRef]
99. Blasco, M.; Gimeno, M.J.; Auqué, L.F. Low temperature geothermal systems in carbonate-evaporitic rocks: Mineral equilibria assumptions and geothermometrical calculations. Insights from the Arnedillo thermal waters (Spain). *Sci. Total Environ.* **2018**, *615*, 526–539. [CrossRef]
100. Franchini, S.; Agostini, S.; Barberio, M.D.; Barbieri, M.; Billi, A.; Boschetti, T.; Pennisi, M.; Petitta, M. HydroQuakes, central Apennines, Italy: Towards a hydrogeochemical monitoring network for seismic precursors and the hydro-seismo-sensitivity of boron. *J. Hydrol.* **2020**, 125754. [CrossRef]
101. Collettini, C.; Cardellini, C.; Chiodini, G.; De Paola, N.; Holdsworth, R.E.; Smith, S.A.F. Fault weakening due to CO_2 degassing in the Northern Apennines: Short- and long-term processes. *Geol. Soc. Lond. Spec. Publ.* **2008**, *299*, 175–194. [CrossRef]
102. Trumpy, E.; Manzella, A. Geothopica and the interactive analysis and visualization of the updated Italian National Geothermal Database. *Int. J. Appl. Earth Obs. Geoinf.* **2017**, *54*, 28–37. [CrossRef]
103. Giggenbach, W.F. Chemical Techniques in Geothermal Exploration. In *D'Amore, F. Applications of Geochemistry in Geothermal Reservoir Development*; UNITAR/UNDP Publication: Rome, Italy, 1991; pp. 119–142.
104. Chatterjee, S.; Sarkar, A.; Deodhar, A.S.; Biswal, B.P.; Jaryal, A.; Mohokar, H.V.; Sinha, U.K.; Dash, A. Geochemical and isotope hydrological characterisation of geothermal resources at Godavari valley, India. *Environ. Earth. Sci.* **2017**, *76*, 97. [CrossRef]
105. Hou, Y.; Shi, Z.; Mu, W. Fluid Geochemistry of Fault Zone Hydrothermal System in the Yidun-Litang Area, Eastern Tibetan Plateau Geothermal Belt. *Geofluids* **2018**, *2018*, 1–13. [CrossRef]
106. Shakeri, A.; Moore, F.; Kompani-Zare, M. Geochemistry of the thermal springs of Mount Taftan, southeastern Iran. *J. Volcanol. Geotherm. Res.* **2008**, *178*, 829–836. [CrossRef]
107. Göb, S.; Loges, A.; Nolde, N.; Bau, M.; Jacob, D.E.; Markl, G. Major and trace element compositions (including REE) of mineral, thermal, mine and surface waters in SW Germany and implications for water–rock interaction. *Appl. Geochem.* **2013**, *33*, 127–152. [CrossRef]
108. Reimann, C.; de Caritat, P. *Chemical Elements in the Environment*; Springer: Berlin/Heidelberg, Germany, 1998; ISBN 978-3-642-72018-5.
109. Morgantini, N.; Frondini, F.; Cardellini, C. Natural trace elements baselines and dissolved loads in groundwater from carbonate aquifers of central Italy. *Phys. Chem. Earth* **2009**, *34*, 520–529. [CrossRef]
110. Bencini, A. Considerazioni sulla distribuzione geochimica del cesio nelle acque termali toscane. *Rend. Della Soc. Ital. Mineral. e Petrologia* **1984**, *39*, 449–454.
111. Boschetti, T.; Venturelli, G.; Toscani, L.; Barbieri, M.; Mucchino, C. The Bagni di Lucca thermal waters (Tuscany, Italy): An example of $CaSO_4$ waters with high Na/Cl and low $CaSO_4$ ratios. *J. Hydrol.* **2005**, *307*, 270–293. [CrossRef]
112. Capecchiacci, F.; Tassi, F.; Vaselli, O.; Bicocchi, G.; Cabassi, J.; Giannini, L.; Nisi, B.; Chiocciora, G. A combined geochemical and isotopic study of the fluids discharged from the Montecatini thermal system (NW Tuscany, Italy). *Appl. Geochem.* **2015**, *59*, 33–46. [CrossRef]
113. Craig, H. Isotopic Variations in Meteoric Waters. *Science* **1961**, *133*, 1702–1703. [CrossRef]
114. Spadoni, M.; Brilli, M.; Giustini, F.; Petitta, M. Using GIS for modelling the impact of current climate trend on the recharge area of the S. Susanna spring (central Apennines, Italy). *Hydrol. Process.* **2010**, *24*, 50–64. [CrossRef]
115. Minissale, A.; Vaselli, O. Karst springs as "natural" pluviometers: Constraints on the isotopic composition of rainfall in the Apennines of central Italy. *Appl. Geochem.* **2011**, *26*, 838–852. [CrossRef]
116. Archer, C.; Noble, P.; Kreamer, D.; Piscopo, V.; Petitta, M.; Rosen, M.R.; Poulson, S.R.; Piovesan, G.; Mensing, S. Hydrochemical determination of source water contributions to Lake Lungo and Lake Ripasottile (central Italy). *J. Limnol.* **2016**. [CrossRef]
117. Gat, J.R.; Carmi, I. Effect of climate changes on the precipitation patterns and isotopic composition of water in a climate transition zone: Case of the Eastern Mediterranean Sea area. In *The Influence of Climate Change and Climatic Variability on the Hydrologic Regime and Water Resources*; International Association Hydrological Sciences Publication Vancouver: Wallingford, UK, 1987; Volume 168, pp. 513–523.
118. Bono, P.; Gonfiantini, R.; Alessio, M.; Fiori, C.; D'Amelio, L. Stable isotopes (d18O, d2H) and tritium in precipitation: Results and comparison with groundwater perched aquifers of Central Italy. In *Isotopic Composition of Precipitation in the Mediterranean Basin in Relation to Air Circulation Patterns and Climate*; TECDOC Series; International Atomic Energy Agency: Vienna, Austria, 2005; Volume 1453, pp. 115–124.
119. Gherardi, F.; Bono, P.; Fiori, C.; Tejeiro, M.D.; Gonfiantini, R. Modeling the altitude isotope effect in precipitations and comparison with the altitude effect in groundwater. In Proceedings of the International Symposium on Advances in Isotope Hydrology and its Role in Sustainable Water Resources Management (IHS-2007), Vienna, Austria, 21–25 May 2007; Volume 21, p. 269.
120. Longinelli, A.; Selmo, E. Isotopic composition of precipitation in Italy: A first overall map. *J. Hydrol.* **2003**, *270*, 75–88. [CrossRef]

121. Celico, P.; Gonfiantini, R.; Koizumi, M.; Mangano, F. Environmental isotope studies of limestone aquifers in central Italy. *Isot. Hydrol.* **1983**, *6*, 173–192.
122. Boschetti, T.; Cifuentes, J.; Iacumin, P.; Selmo, E. Local Meteoric Water Line of Northern Chile (18° S–30° S): An Application of Error-in-Variables Regression to the Oxygen and Hydrogen Stable Isotope Ratio of Precipitation. *Water* **2019**, *11*, 791. [CrossRef]
123. Zuppi, G.M.; Bortolami, G. Hydrogeology: A privileged field for environmental stable isotopes applications. *Some Italian examples. Rend. Della Soc. Ital. Mineral. Petrologia* **1982**, *38*, 1197–1212.
124. Romano, E.; Preziosi, E. Precipitation pattern analysis in the Tiber River basin (central Italy) using standardized indices: Precipitation pattern analysis in the tiber river basin. *Int. J. Climatol.* **2013**, *33*, 1781–1792. [CrossRef]
125. Burnard, P.; Bourlange, S.; Henry, P.; Geli, L.; Tryon, M.D.; Natal'in, B.; Sengör, A.M.C.; Özeren, M.S.; Çagatay, M.N. Constraints on fluid origins and migration velocities along the Marmara Main Fault (Sea of Marmara, Turkey) using helium isotopes. *Earth Planet. Sci. Lett.* **2012**, *341–344*, 68–78. [CrossRef]
126. O'Nions, R.K.; Oxburgh, E.R. Helium, volatile fluxes and the development of continental crust. *Earth Planet. Sci. Lett.* **1988**, *90*, 331–347. [CrossRef]
127. Caracausi, A.; Martelli, M.; Nuccio, P.M.; Paternoster, M.; Stuart, F.M. Active degassing of mantle-derived fluid: A geochemical study along the Vulture line, southern Apennines (Italy). *J. Volcanol. Geotherm. Res.* **2013**, *253*, 65–74. [CrossRef]
128. Sano, Y.; Gamo, T.; Williams, S.N. Secular variations of helium and carbon isotopes at Galeras volcano, Colombia. *J. Volcanol. Geotherm. Res.* **1997**, *77*, 255–265. [CrossRef]
129. Martelli, M.; Nuccio, P.M.; Stuart, F.M.; Di Liberto, V.; Ellam, R.M. Constraints on mantle source and interactions from He-Sr isotope variation in Italian Plio-Quaternary volcanism: Italian plio-quaternary volcanism. *Geochem. Geophys. Geosyst.* **2008**, *9*, 1–16. [CrossRef]
130. Cardello, G.L.; Consorti, L.; Palladino, D.M.; Carminati, E.; Carlini, M.; Doglioni, C. Tectonically controlled carbonate-seated maar-diatreme volcanoes: The case of the Volsci Volcanic Field, central Italy. *J. Geodyn.* **2020**, *139*, 101763. [CrossRef]
131. Ballentine, C.J.; Marty, B.; Lollar, B.S.; Cassidy, M. Neon isotopes constrain convection and volatile origin in the Earth's mantle. *Nature* **2005**, *433*, 6. [CrossRef] [PubMed]
132. Graham, D.W. Noble Gas Isotope Geochemistry of Mid-Ocean Ridge and Ocean Island Basalts: Characterization of Mantle Source Reservoirs. *Rev. Mineral. Geochem.* **2002**, *47*, 247–317. [CrossRef]
133. Sano, Y.; Marty, B. Origin of carbon in fumarolic gas from island arcs. *Chem. Geol.* **1995**, *119*, 265–274. [CrossRef]
134. Sharp, Z. *Principles of Stable Isotope Geochemistry*, 2nd ed.; The University of New Mexico: Albuquerque, NM, USA, 2017. [CrossRef]
135. Pistiner, J.S.; Henderson, G.M. Lithium-isotope fractionation during continental weathering processes. *Earth Planet. Sci. Lett.* **2003**, *214*, 327–339. [CrossRef]
136. Teng, F.Z.; McDonough, W.F.; Rudnick, R.L.; Wing, B.A. Limited lithium isotopic fractionation during progressive metamorphic dehydration in metapelites: A case study from the Onawa contact aureole, Maine. *Chem. Geol.* **2007**, *239*, 1–12. [CrossRef]
137. Mathurin, F.A.; Drake, H.; Tullborg, E.-L.; Berger, T.; Peltola, P.; Kalinowski, B.E.; Åström, M.E. High cesium concentrations in groundwater in the upper 1.2km of fractured crystalline rock—Influence of groundwater origin and secondary minerals. *Geochim. Cosmochim. Acta* **2014**, *132*, 187–213. [CrossRef]